Earth-Science Reviews 179 (2018) 372–391

Contents lists available at ScienceDirect

Earth-Science Reviews

journal homepage: www.elsevier.com/locate/earscirev

Productivity changes across the mid-Pleistocene climate transition

Liselotte Diester-Haass[a,*], Katharina Billups[b], Caroline Lear[c]

[a] Universität des Saarlandes, Zentrum für Umweltforschung, 66041 Saarbrücken, Germany
[b] School of Marine Science and Policy, University of Delaware, 700 Pilottown Road, Lewes, DE 19958, USA
[c] School of Earth and Ocean Sciences, Cardiff University, Main Building, Park Place, Cardiff CF10 3AT, UK

ARTICLE INFO

Keywords:
Paleoceanography
Mid-Pleistocene climate transition
Benthic foraminifera
Paleoproductivity
Biological pump

ABSTRACT

We use benthic foraminiferal accumulation rates as a proxy for productivity changes during the mid-Pleistocene climate transition (MPT) (~1.2 Ma to 0.4 Ma). Our data are chosen to test the hypothesis that longer-term cooling and the onset of 100 kyr cyclicity are linked to atmospheric CO_2 draw-down associated with an increase in primary productivity. To this end, we have constructed records from a global array of seven sites spanning major ocean basins and representing different hydrographic regimes (e.g., high and low latitudes, upwelling versus the deep western warm pools). We compare our data to published productivity proxy records from each site to identify limitations and uncertainties in the reconstructions. Results indicate that there is evidence for productivity increases during the onset of the MPT (1.2–1.0 Ma), but the changes are not globally synchronous and likely reflect regional hydrographic variability. On the orbital scale, productivity maxima tend to occur more closely related to glacial than interglacial intervals overall, but the relationships are not consistent. High interglacial productivity characterizes low latitude sites some of the time. In the obliquity band, high interglacial productivity in the eastern equatorial Pacific coincides with low interglacial productivity in the Southern Ocean, supporting a high to low latitude link via intermediate water circulation distribution of nutrients. On the regional scale, our records contribute new evidence for changes in Northern Hemisphere frontal systems during the MPT and for a close link between surface ocean production of organic matter and consumption on the ocean floor in the western tropical Atlantic. Pyrite counts at the two Southern Ocean sites provide supporting evidence for sluggish thermohaline overturn during the mid-point of the MPT at ~900 ka. Taken together, our records do not show a globally synchronous productivity signal that would support the biological pump as a driver for potential CO_2-induced climate cooling during the MPT. Instead, we document complex regional variations in the carbon cycle, reflecting a combination of both biological and physical processes both on the longer as well as on the orbital time-scale.

1. Introduction

The mid-Pleistocene climate transition (MPT) marks the evolution of asymmetric climate cycles defined by slow expansion of continental ice sheets toward mid latitudes followed by rapid melting culminating in interglacial warmth. As outlined by oxygen isotope records, the transition began roughly 1.2 Ma when climate cycles directly responded to orbitally driven insolation changes (41 kyr obliquity and 23 kyr precession cycles, Fig. 1). By ~0.95–0.9 Ma, climate cooling reached new extremes, and by ~0.6 Ma, climate changes followed an apparent ~100 kyr pacing of glacial and interglacial extremes that cannot be explained by changes in insolation directly (e.g., Hays et al., 1976; Mudelsee and Schulz, 1997).

Several hypotheses have been proposed to explain this climate system nonlinearity, but as of yet none sufficiently explain its origins (e.g., see recent reviews by Clark et al., 2006; McClymont et al., 2013). To summarize, Imbrie et al. (1993) were the first to emphasize the importance of feedbacks between poleward heat transport (termed the Nordic Heat Pump in their model) and meridional overturning as a key driver of the 100 kyr climate pattern. With a geologic focus, Clark and Pollard (1998) discuss the exposure of crystalline basement providing an increasingly more solid footing allowing the accumulation of thicker ice sheets on Northern Hemisphere continents. Elderfield et al. (2012) provide evidence against slow cooling but for an abrupt increase in glacial Antarctic ice volume during the mid-point of the MPT at 0.9 Ma. More recently Pena and Goldstein (2014) provide new geochemical data indicating changes in meridional overturning circulation at 0.9 Ma. Lear et al. (2016) contribute supporting evidence for deep ocean carbon sequestration as an amplifier of the 100 kyr climate cycle at this time. Emphasizing the role of climate thresholds, most recently,

* Corresponding author.
E-mail addresses: l.haass@mx.uni-saarland.de (L. Diester-Haass), kbillups@udel.edu (K. Billups), LearC@cardiff.ac.uk (C. Lear).

https://doi.org/10.1016/j.earscirev.2018.02.016
Received 9 July 2017; Received in revised form 16 February 2018; Accepted 16 February 2018
Available online 27 February 2018

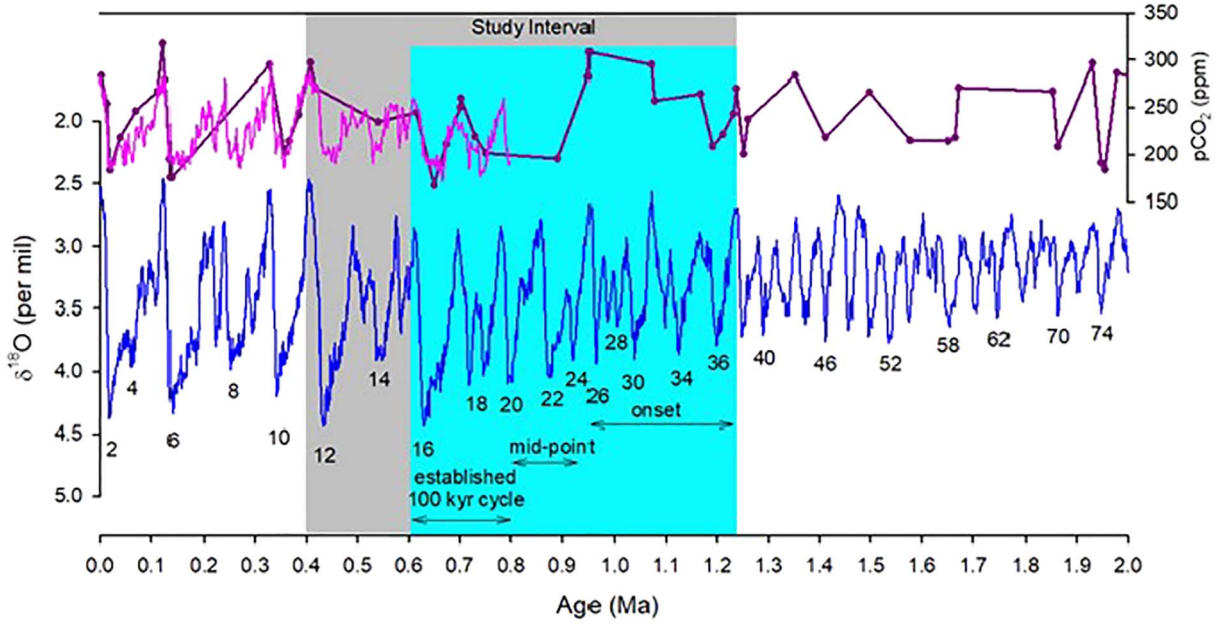

Fig. 1. Benthic foraminiferal $\delta^{18}O$ record (blue curve,) and atmospheric CO_2 levels (purple and red curves) spanning the past 2 myr. The mid-Pleistocene Transition (blue box) is delineated by increasingly more extreme $\delta^{18}O$ maxima (glacial Marine Isotope Stages, MIS, are labeled; Lisiecki and Raymo, 2005) and their 100 kyr pacing between 1.2 Ma and 0.6 Ma. MIS 24-21 are considered the mid-point of the transition (Mudelsee and Schulz, 1997). The grey box outlines our study interval (~0.4–1.2 Ma). The purple curve reflects CO_2 reconstruction based on the boron isotopic composition of foraminifera (Hönisch et al., 2009), the red curve represents CO_2 measurements from ice cores (Lüthi et al., 2008).

Tzedakis et al. (2017) propose that the 100 kyr cycle reflects a weakened response to some insolation maxima, thereby prolonging the ice growth phase.

Although a plausible climate forcing factor (e.g., Herbert et al., 2010), the role of CO_2 in mediating the MPT is equivocal. Continuous ice-core records do not span the entire transition interval (Lüthi et al., 2008; Wolff et al., 2010). Geochemical proxies only resolve generally higher minimum, presumably glacial, CO_2 levels pre MPT (Hönisch et al., 2009, Fig. 1). Pacific-Atlantic benthic foraminiferal $\delta^{13}C$ differences have been interpreted to indicate a unique CO_2 minimum at 920 ka, but these records do not show a long-term permanent decrease across the entire transition interval (Lisiecki, 2010).

Here we investigate the extent to which changes in the biological pump may support CO_2 as a forcing mechanism for the climatic cooling that defines the MPT. Marine primary productivity depends on insolation, incident light levels, and nutrient availability, potentially representing an important feedback in the climate system through its impact on the global carbon cycle. To this end, we have identified seven sites with different hydrographic regimes, and where possible, we assess the evolution of orbital pacing of productivity in each region (Fig. 2, Table 1). Our main proxy is the accumulation of benthic foraminifera because these organisms feed on organic detritus synthesized in the photic zone and exported to the sea bed. They should thus be sensitive to variations in the local biological pump, yet be less sensitive to changes in bottom water organic carbon content caused by deep water circulation (e.g., Berger and Wefer, 1990; Herguera and Berger, 1991; Nees, 1997; Schmiedl and Mackensen, 1997; Yasuda, 1997; van der Zwaan et al., 1999; Herguera, 2000; Diester-Haass et al., 2004). Benthic foraminiferal accumulation rates resolve marine productivity signals during major climate transitions such as the Oligocene/Miocene boundary (Diester-Haass et al., 2011), the mid-Miocene climatic optimum (Diester-Haass et al., 2009, 2013) and the late Miocene (Diester-Haass et al., 2006). In addition to benthic foraminifera, we use other faunal indicators of various aspects of the marine carbon cycle and productivity, such as the accumulation of radiolaria as a proxy for productivity in the photic zone (e.g., Takahashi, 1987; Lazarus et al., 2006, 2008) and a planktic foraminiferal fragmentation index as an indicator of deep water corrosivity in response to, presumably, respired CO_2 content (e.g., Lee and Shackleton, 1992). As pertinent to individual sites, we also counted ice rafted debris (IRD), monitored the Fe content of sediments as an indicator of eolian inputs to the North Atlantic, and we counted pyrite as a sediment redox indicator in the Southern Ocean. To place our records into a larger context, we compare the new data with previously published records of productivity based on other proxies (e.g., biogenic opal and alkenone mass accumulation rates).

2. Methods

2.1. Site selection strategy

We have selected seven sites to represent a broad range of hydrographic regimes, with different local and regional controls on productivity (Fig. 2 and Table 1). Briefly, the highest latitude sites come from the Atlantic Ocean and display the largest seasonal productivity differences controlled by variations in seasonal insolation and the migration of frontal systems (Deep Sea Drilling Project, DSDP, Sites 552A and 607). Productivity variations at tropical Ocean Drilling Program (ODP) Sites 925, 849, and 806 are controlled by changes in mixed layer depth and upwelling. Southern Ocean ODP Sites 1090 and 1123 underlie modern day high nitrate, low chlorophyll regions where productivity is limited by Fe. Together, these sites from vastly different regimes allow us to investigate whether there was a globally coherent whole ocean change in productivity or whether regional hydrographic changes dominate the system during the MPT.

2.2. Sampling and micropalaeontological counts

At each site, the MPT study interval was identified from published stable isotope records (Table 1). To the extent possible, each site was sampled from the same cores as the published data. The sample interval was chosen to achieve at a temporal resolution of 3–5 kyr to fully resolve long-term trends as well as glacial to interglacial variability in paleoproductivity.

Sample processing followed standard procedures including oven drying overnight and wet sieving to obtain the > 63 μm size fraction. Samples were then dry-sieved into sub-fractions (63–125, 125–250,

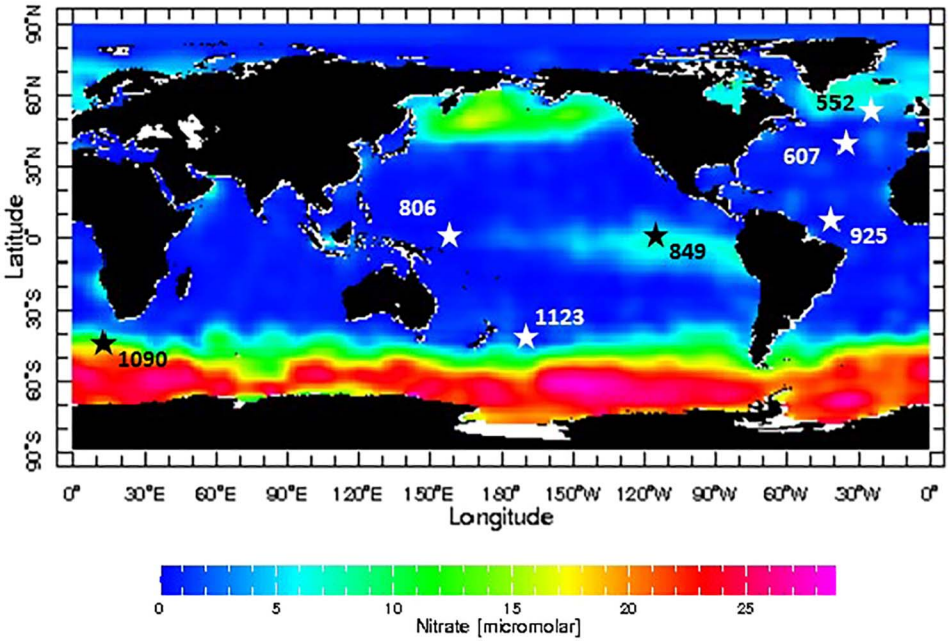

Fig. 2. Locations of study sites on a map of nitrate concentrations. The map was generated using the Lamont Doherty Climate Data Library. The study sites sample different hydrographic regimes spanning relatively stable equatorial regions (Sites 925, 806), equatorial upwelling (Site 849), North Atlantic subtropical gyre margin (Site 607) and high latitudes (Site 552), and the Southern Ocean (Site 1090, Site 1123). Table 1 provides the precise location and summarizes modern seasonal productivity range.

Table 1
Summary of site locations and modern seasonal productivity ranges.

Site	Source[a]	Water depth (m)	Latitude	Longitude	Modern productivity (g C m^{-2} season^{-1})[b]
552	1	2315	56°N	23°W	9–72
607	2	3427	41°N	33°W	9–72
925	3	3042	4°N	43°W	18–32
1090	4	3060	43°S	9°E	9–32
1123	5	3290	42°S	171°W	18–50
849	6	3851	0°N	111°W	27–50
806	7	2532	0°N	159°E	27–50

[a] Numbers refer to the following stable isotope data and age model sources: 1-Raymo et al. (1990) for both; 2-Lear et al. (2016)/Lisiecki and Raymo (2005); 3-Bickert et al. (1997)/Lisiecki and Raymo (2005); 4-Martinez-Garcia et al. (2011) for both; 5-Elderfield et al. (2012) for both; 6-Mix et al. (1995) for both; 7-Karas et al. (2009) for both.
[b] Antoine et al. (1996).

250–500, > 500 μm) for sedimentological-micropaleontological studies. In each fraction, 800 grains (if present) were counted and various biogenic (including whole planktic tests and test fragments), clastic, and authigenic components were differentiated to yield percentage composition of the sand fraction. The numbers of benthic foraminifera in the fractions > 150 μm were summed and divided by the weight of the > 150 μm sample to give the number of benthic foraminifera per gram of total sediment. All data are archived electronically at the NOAA World Data Center-A for Paleoclimate (https://www.ncdc.noaa.gov/data-access/paleoclimatology-data).

2.3. Sedimentary iron content

At Site 607, XRF Core Scanner Fe and other elemental data were collected every two cm down-core over a one cm^2 area. Here we report the Fe/Ca ratios. The down-core slit size was 10 mm using generator settings of 10 kV, a current of 200 mA, and a sampling time of 15 s directly at the split core surface of the archive half with XRF Core Scanner II (AVAATECH Serial No. 2) at the MARUM, University of Bremen. The split core surface was covered with a four micron thin SPEXCerti Prep Ultralene1 foil to avoid contamination of the XRF measurement unit and desiccation of the sediment. The data reported here were acquired by a Canberra X-PIPS Silicon Drift Detector (SDD; Model SXD 15C-150-500) with 150 eV X-ray resolution, the Canberra Digital Spectrum Analyzer DAS 1000, and an Oxford Instruments 50 W XTF5011 X-Ray tube with rhodium (Rh) target material. Raw data spectra were processed by the analysis of X-ray spectra by Iterative Least square software (WIN AXIL) package from Canberra Eurisys.

2.4. Age models

The age models from each study site are based on oxygen isotope stratigraphy and are published in the literature (Table 1). With the exception of Site 806, these age models have been placed on orbitally-tuned time-scales consistent with the $\delta^{18}O$ stack of Lisiecki and Raymo (2005) (LR04). For Site 806 we use the more recent age model of Karas et al. (2009) as it avoids spurious changes in sedimentation rates at the site (Bickert, personal communication, 2016). To facilitate the description and discussion of the results, we use the individual $\delta^{18}O$ record at each site to identify the Marine Isotope Stages (MIS). We point out that the Site 607 benthic foraminiferal stable isotope record was generated in the context of a companion study (Lear et al., 2016), and hence from the same sample intervals as the faunal data shown here (Lear et al., 2016).

2.5. Benthic foraminiferal-derived paleoproductivity

We derive benthic foraminiferal accumulation rates (BFAR) by multiplying the number of benthic foraminiferal tests in a sample by the dry bulk density (DBD) of the sediment and the linear sedimentation rates (LSR). This approach accounts for the effect of increases or decreases in the other sediment components on the relative amount of benthic foraminifera found in a sample. The dry bulk density (DBD) for DSDP Sites 552 and 607 is calculated using wet bulk density (WBD) and porosity (P) data (DBD = WBD − 1.026 ∗ P/100) published in the shipboard literature for each site (Ruddiman et al., 1987; Roberts et al., 1984, respectively). For ODP sites, DBD values are published in the pertinent shipboard literature. Linear sedimentation rates are derived from the age-depth relationships at each site. To then calculate paleoproductivity, we use the empirical relationship between BFAR from core top sediments from the equatorial Pacific and Atlantic and the corresponding organic carbon flux of Herguera (2000) (Eq. (1)):

$$pProd = 0.4 * Z * BFAR^{0.5} \quad (1)$$

where pProd stands for paleoproductivity, Z is the water depth of the

sample, and BFAR are the benthic foraminiferal accumulation rates.

There are some uncertainties with this approach. Fundamentally, mass accumulation derived proxies are always a function of linear sedimentation rates and therefore depend on the age model. As age models utilize orbital tuning, the resolution of age-depth point for LSR is relatively high, about 20 kyr. The DBD data, however, have lower resolution and may underestimate glacial to interglacial variability. Furthermore, the abundance of benthic foraminiferal tests can be influenced by dissolution of less resistant planktonic foraminiferal tests. To identify this potential bias, we evaluate corresponding variations in the foraminiferal fragmentation index, which is the ratio of test fragments with respect to the total abundance of fragments and whole planktic foraminiferal tests in a sample (e.g., Diester-Haass et al., 2009).

Conceptually, the transfer of organic matter from the surface to the deep ocean, the biological pump, is complex and what reaches the ocean floor may not directly reflect the magnitude of primary productivity at the sea surface (Lampitt and Anita, 1997). An important control may be the phytoplankton community structure (e.g., carbonate versus silica producers), which determines at what depth organic carbon can sink before it is remineralized (Boyd and Newton, 1999; Francois et al., 2002). Therefore, we also counted numbers of *Uvigerina* species, benthic foraminifera typical for a near surface infaunal habitat, that are correlated to high nutrient supply, i.e. high accumulation rates of organic matter (Lutze, 1980; Miller and Lohmann, 1982; Lutze and Coulbourn, 1984). Hence, our strategy is to compare available productivity proxies at each site.

2.6. Time series analysis

We use time series analysis to establish the significance of orbital-scale glacial to interglacial productivity variations at those sites where the records are continuous and the temporal resolution is sufficiently high (Sites 925, 1090, 1123, and 849). These results are summarized in Table 2. In addition, we use iterative cross-spectral analyses between benthic foraminiferal $\delta^{18}O$ values and productivity to investigate potential changes in the relationship on glacial to interglacial time scales across the MPT. For this purpose, we focus on two segments, one before (800–1200 ka) and one after the mid-point of the MPT (400–800 ka; Table 3).

Cross-spectral analyses are conducted using the ARAND software package (Howell, 2012). Records are linearly detrended and interpolated at 3 kyr (Site 925), 3.4 kyr (Site 1090 and 1123), and 4 kyr (Site 849) intervals to approximate the original sampling resolution of the proxies. At Site 925, we also use cross spectral analysis to confirm a correlation between productivity and surface water nutrient content as measured by relative abundance of *Florisphaera* at Site 925 (Bassinot et al., 1997). Data were interpolated using the same 3 kyr time step.

3. Results

3.1. Subpolar North Atlantic DSDP Site 552

At 56°N and 23°W, Site 552 (Fig. 2) underlies the North Atlantic Drift well to the south of the modern-day position of the Arctic Polar Front (Roberts et al., 1984). Present-day primary productivity ranges from about 9 to 72 g C m^{-2} $season^{-1}$ (Antoine et al., 1996; Table 1) with maximum productivity during the spring bloom. At ~2300 m depth, the site lies in the path of waters spilling through the Gibbs Fracture Zone (primarily Norwegian Sea Overflow but also Mediterranean Overflow). Stable isotope data from this site contributed to one of the first syntheses of mid-Pleistocene climate change and deep water circulation (Raymo et al., 1990). The relatively small variability in benthic foraminiferal $\delta^{13}C$ values attests to the general lack of a glacial to interglacial deep water circulation signal at this site (Raymo et al., 1990) (Fig. 3a and b). However, the $\delta^{13}C$ minimum characterizing the mid-Pleistocene during MIS 22 (880 ka) is distinctly evident in the record.

Benthic foraminiferal accumulation rate-derived paleoproductivity increases during the onset of the MPT (MIS 35-28), displays a distinct maximum during MIS 28, decreases toward MIS 24, and then remains low during the MPT mid-point (MIS 24-20) (Fig. 3c). These productivity trends are supported by the benthic foraminiferal test counts, which show a long-term increase between MIS 35 and MIS 30 and a decrease toward MIS 24 (Fig. 3e). Thus, only the absolute magnitude of the productivity maximum during MIS 28 may be a function of the LSR multiplier as LSR display a distinct maximum at that time (Fig. 3d).

Distinct productivity maxima, supported by maxima in test counts, occur during glacial (MIS 34, 30, 28, 24) as well as interglacial (MIS 33, 31, 27) stages (Fig. 3c and e). After MIS 22, the pattern is more difficult to recognize, but glacial extremes tend to be associated with low benthic foraminiferal numbers (MIS 18, 16, 14). Enhanced productivity during interglacial intervals throughout the entire mid-Pleistocene interval is supported by peaks in *Uvigerina* and radiolarian abundances (Fig. 3f and g, respectively). The fragmentation index also shows distinct maxima primarily during interglacial intervals (Fig. 3h). The association between high benthic foraminiferal and radiolarian abundances and fragmentation maxima during interglacial intervals suggests a link between surface water nutrients and in situ respiration of organic matter in the bottom waters.

The long-term trend in the alkenone MAR record from nearby Site 982 (Fig. 3i) generally agrees with the long-term trend in the benthic foraminiferal-derived productivity. Alkenone MARs increase during the onset of the MPT (MS 35-27) and display a minimum during the mid-point (MIS 24-22). Consistent with *Uvigerina*, radiolarian, and fragmentation patterns, the alkenone derived productivity maxima appear to occur during interglacial intervals, particularly after MIS 22.

The IRD component of Site 552 sediments shows distinct maxima during glacial intervals (Fig. 3j), an observation that agrees with prior studies of the region (e.g., Hernandez-Almeida et al., 2013). The two glacial intervals of the mid-point of the MPT (MIS 24-22) display the highest IRD peaks of the entire study interval dominating the sediment lithology at those times (> 50%).

We note that relatively large fluctuations in the IRD component may

Table 2
Average phase and phase error in degrees for significant (> 80%) coherence (k) between $-\delta^{18}O$[a] and productivity derived from benthic foraminiferal accumulation rates. Values of k are in parentheses.

Site	~100 kyr	41 kyr	23–19 kyr
925	−24 ± 32° (0.50)[b]	−106 ± 30° (0.57)	–
1090	103 ± 27° (0.62)	–	−131 ± 26° (0.64)
1123	155 ± 30° (0.53)	−170 ± 27° (0.57)	170 ± 22° (0.65)
849	–	85 ± 17° (0.75)	140 ± 20° (0.65)

[a] Multiplied by −1 in order to reference interglacial intervals.
[b] Periodicity is 208 kyr.

Table 3
Phase relationships for $-\delta^{18}O$[a] versus productivity for those significant above the 80% from iterative cross spectral analysis.

Site	Time interval (ka)	100 kyr	41 kyr	23 kyr/19 kyr
925	433–800	−118 ± 27°	−53 ± 26°	45 ± 35°/−10 ± 27°
	800–1165	–	−133 ± 29°	−140 ± 36°
1090	581–901	121 ± 20°	–	–
	901–1220	–	–	–
1123	422–811	132 ± 19°	–	–
	811–1200	–	−119 ± 25°	−148 ± 23°
849	340–755	–	99 ± 20°	135 ± 23°
	755–1170	–	63 ± 17°	165 ± 17/137 ± 21°

[a] Multiplied by −1 in order to reference interglacial intervals.

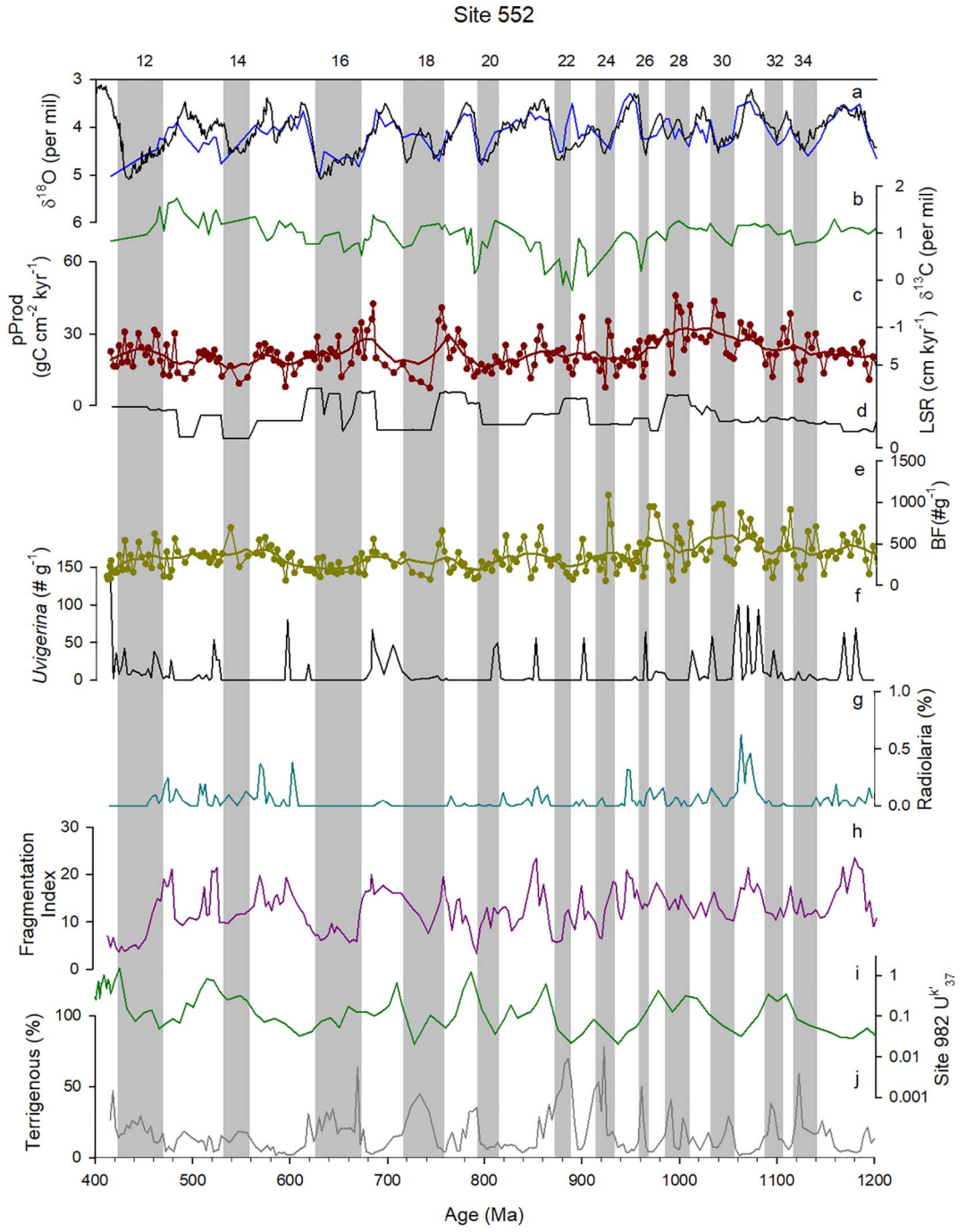

Fig. 3. Summary of results from North Atlantic Site 552. Benthic foraminiferal $\delta^{18}O$ (a) and $\delta^{13}C$ (b) records from Raymo et al. (1990). Black line in panel (a) shows the global $\delta^{18}O$ stack of Lisiecki and Raymo (2005). Benthic foraminiferal-derived paleoproductivity (c), linear sedimentation rates (LSR) (d), benthic foraminiferal test counts per gram sediment (e), number of *Uvigerina* per gram sediment (f), percent radiolaria (g), fragmentation index (see text) (h), alkenone mass accumulation rates ($U^{k'}_{37}$ index) from Site 982 (Lawrence et al., 2010) (i); percent ice rafted debris (IRD) (j).Vertical grey boxes highlight glacial Marine Isotope Stages, after Lisiecki and Raymo (2005).

have affected the relative abundance of other sediment constituents, the so-called closed sum problem. For instance, maxima in the IRD counts correspond precisely to minima in the benthic foraminiferal test counts (Fig. 3i and e, respectively). Thus, interpretations of the absolute values of the productivity reconstructions are limited. The relative changes, however, are likely robust, and are supported by the alkenone MARs.

3.2. North Atlantic DSDP Site 607

North Atlantic Site 607 (41°N, 33°W, Fig. 2) underlies the northern edge of the subtropical gyre on the western flank of the Mid Atlantic Ridge (Ruddiman et al., 1987). Surface hydrography is thus associated with seasonal variations in the position of the northern limb of the subtropical gyre and the strength of the Gulf Stream, which is strongest during the fall and weakest during the spring (Hogg and Jones, 1995). The annual primary productivity range is comparable to that at Site 552 (~9–72 g C m^{-2} $season^{-1}$) being low during the fall and winter and high during the spring and summer (Antoine et al., 1996; Table 1).

At ~3400 m water depth, Site 607 lies in the core of North Atlantic Deep Water (NADW) as it enters the Atlantic Ocean. The position of the site has been highly sensitive to glacial/interglacial changes in deep water circulation since the early Pleistocene (Lang et al., 2016). It is

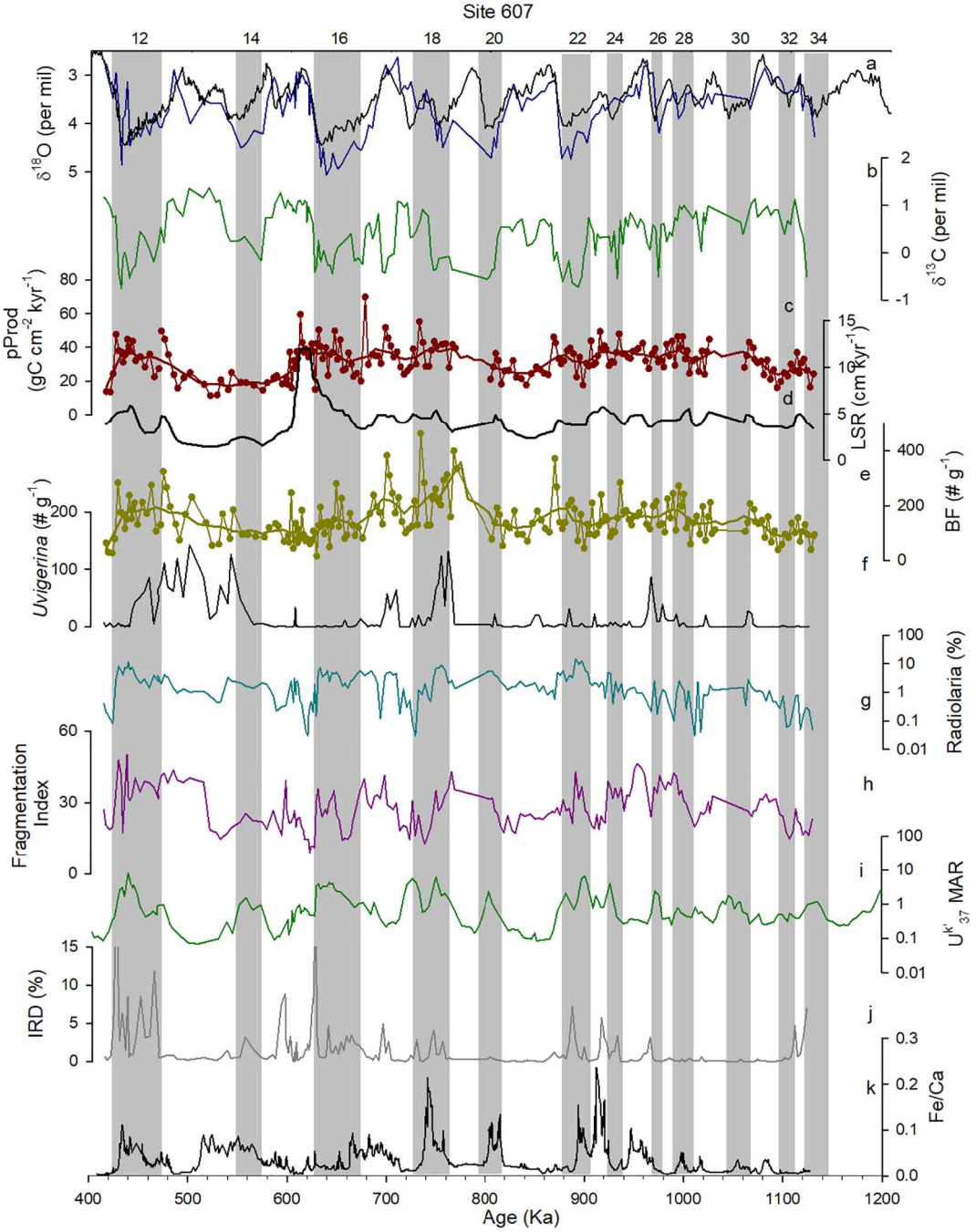

Fig. 4. Summary of results from North Atlantic Site 607. Benthic foraminiferal $\delta^{18}O$ (a) and $\delta^{13}C$ (b) from Lear et al. (2016); Black line in panel (a) shows the global $\delta^{18}O$ stack of Lisiecki and Raymo (2005). Benthic foraminiferal-derived paleoproductivity (c), linear sedimentation rates (LSR) (d), benthic foraminiferal test counts per gram sediment (e), number of *Uvigerina* per gram sediment (f), percent radiolaria (g), fragmentation index (see text) (h), alkenone mass accumulation rates ($U^{k'}_{37}$ index) (Lawrence et al., 2010) (i); percent ice rafted debris (IRD) (i); XRF based Fe counts in bulk sediments (k). Vertical grey boxes highlight the timing of glacial Marine Isotope Stages after Lisiecki and Raymo (2005).

also well established that the relative amount of corrosive Antarctic Bottom Water (AABW) increased during the glacial intervals of the MPT (e.g., Raymo et al., 1990; Ferretti et al., 2005; Poirier and Billups, 2014). This pattern is evident from the stable isotope records that show a close relationship between low $\delta^{18}O$ values and high $\delta^{13}C$ values and vice versa (Fig. 4a and b, respectively). The $\delta^{13}C$ record shows a larger amplitude than the record at more northern Site 552, primarily due to more extreme $\delta^{13}C$ minima (Fig. 4b). This observation attests to the dominance of AABW during glacial intervals, particularly during MIS 22 and thereafter (Raymo et al., 1990; Poirier and Billups, 2014; Lang et al., 2016).

As at North Atlantic Ocean Site 552, benthic foraminiferal-derived paleoproductivity shows a gradual increase during the onset of the MPT (MIS 34-28), but here productivity remains constant thereafter and does not decrease until after MIS 23 (Fig. 4c). Linear sedimentation rates parallel the long-term productivity trends, but benthic foraminiferal test counts support a productivity increase between MIS 34 and MIS 28 and a maximum during the MIS 22/21 transition. Furthermore, benthic foraminiferal numbers are consistent with relatively low productivity early during MIS 22 and throughout MIS 21 (Fig. 4e). At the finer scale, no clear glacial to interglacial variability in benthic foraminiferal-derived paleoproductivity exists at this site.

Other faunal indicators also show a complex pattern. *Uvigerina* do not display any long-term trends, but show high numbers during glacial

MIS 18, 14, and 12, as well as interglacial MIS 17 and 13 (Fig. 4f). Radiolaria generally increase during the onset of the MPT reaching a distinct maximum during MIS 22 (Fig. 4g). Other abundance maxima tend to fall during glacial intervals as well. Planktic foraminiferal test fragmentation evidences increased dissolution during the onset of the MPT (MIS 34-25), with distinct maxima occurring during glacial (MIS 28-26, 22, 20, 16, and 12) as well as some interglacial (MIS 31, 27 and 25, 17, 15, 13) intervals (Fig. 4h). Thus, the two latter two curves might support a top to bottom link between respiration and dissolution during the onset of the MPT and during MIS 22.

Alkenone MARs from this site (Fig. 4i; Lawrence et al., 2013) differ from those at Site 982 (Fig. 3i) in that there is no long-term increase during the onset of the MPT and a distinct maximum occurs between MIS 24 and MIS 22, a time of minimal accumulation at Site 982. Similar to the other records at Site 607, however, there is a distinct minimum during MIS 21 (compared to a maximum at Site 982). At the fine scale, a double alkenone MAR peak characterizes MIS 22, akin to a similar double maximum in radiolarian abundance and planktic foraminiferal fragmentation and thus supports the notion of a top to bottom link via productivity and respiration at this time.

Two measures of terrigenous sediment inputs are provided by counts of IRD in the processed samples (Fig. 4j) and by Fe/Ca ratios in bulk sediment (Fig. 4k). The IRD counts are low (below 10%, Fig. 4j) and thus not likely to have had a significant impact on the variations in the other sediment components. Although low overall, increasingly higher IRD maxima occur during the glacial MIS 26, 24 and 22 with highest and most frequent IRD peaks during MIS 12. Fe/Ca ratios remain relatively constant during the onset of the MPT and begin to display increasingly larger maxima after MIS 26 (Fig. 4k). As is the case with some of the other proxies, individual Fe/Ca peaks occur during glacial (MIS 30, 28, 22, 20, 18, and 12) as well as interglacial (MIS 31, 25, 23, 17, 15) intervals throughout. Thus, there is only little correspondence between the two terrigenous components. The Fe record differs enough from the IRD record to indicate that Fe content has a different source, such as from eolian input in addition to, or instead of, Fe-bearing minerals brought in via IRD.

3.3. Northwestern tropical Atlantic Ocean ODP Site 925

Site 925 (4°N, 43°W, Fig. 2) lies on Ceara Rise in the northwestern tropical Atlantic Ocean (Curry et al., 1995). The surface and upper water column hydrography are governed by seasonal variations in the relative strength of the southeastern trade winds and the position of the Intertropical Convergence Zone (ITCZ) (e.g., Philander and Pacanowski, 1986). Although the mixed layer depth varies, the upper water column remains stratified to at least 50 m and productivity remains relatively constant throughout the year (18–32 g C m^{-2} season^{-1}, Antoine et al., 1996; Table 1). The higher productivity occurs during the fall and winter when the thermocline is shallower due to divergence underneath the low-pressure cell of the ITCZ.

At 3042 m water depth, Site 925 lies within modern NADW above the mixing zone with AABW. Akin to Site 607, Site 925 benthic foraminiferal $\delta^{13}C$ values show pronounced minima during glacial intervals, particularly MIS 22 (Fig. 5a and b) (Bickert et al., 1997). In fact, glacial versus interglacial snapshots of $\delta^{13}C$ values illustrate that the two sites have a very similar deep water mass history (Poirier and Billups, 2014).

Benthic foraminiferal-derived paleoproductivity shows longer-term modulation in its average values (Fig. 5c). Productivity appears to increase in the earliest portion of the record (MIS 35-31), but a unidirectional trend toward increasing or decreasing values is not apparent in the data. Instead, regular cyclicity, outlined by multiple data points, characterizes the record (Fig. 5c). Productivity maxima occur during glacial (e.g., MIS 30, 28, 26, 18, 16, 14) as well as interglacial (MIS 31, 23, 19, 15, 13) intervals.

These trends appear to be a robust paleoenvironmental signal as they are largely independent of the linear sedimentation rates (Fig. 5d), and they are mimicked by the number of benthic foraminiferal tests per gram sediment (Fig. 5e). *Uvigerina* counts are relatively low, < 50 tests per gram sediment (Fig. 5f), as expected under an oligotrophic region of the ocean. Accordingly, radiolaria are rare in these sediments (not plotted). The fragmentation index displays maxima that lie within glacial (MIS 28, 26, 22, 20, 16) as well as interglacial (MIS 33, 27, 25, 21) intervals (Fig. 5g). However, it does not appear that enhanced planktic foraminiferal test dissolution has consistently biased the benthic foraminiferal-derived productivity record toward maxima because at the finer-scale, fragmentation maxima do not coincide with productivity maxima and vice versa (Fig. 5c versus g).

Time series analysis indicates that productivity changes reflect orbital-scale variability. Significant coherence exists between $\delta^{18}O$ values and productivity at a longer, perhaps eccentricity-related band, and at obliquity (Table 2). Iterative cross-spectral analyses illustrate that coherence at the 100 kyr cycle becomes significant after 800 ka, and the relatively long phase angle ($-118 \pm 27°$) suggests that maxima occur in closer association with glacial than with interglacial maxima (Table 3). In the obliquity band, the phase angle changes. During the older time interval (800–1200 ka) productivity is closer in timing with glacial maxima while it is closer in timing with interglacial maxima during the younger time slice (400–800 ka) (Table 3). Similarly, in the precession band, which is significant in the iterative mode, the phase relationships change across the mid-point of the MPT switching from productivity maxima near glacial to more interglacial timing (Table 3).

At Site 925, orbital-scale variations in benthic foraminiferal-derived productivity can be compared with relative abundances of the coccolithophore *Florisphaera profunda* (Bassinot et al., 1997) (Fig. 5h). *Florisphaera* abundance variations reflect shifts in the coccocolith species assemblages in response to changes in the depth of the nutricline and hence reflect changes in upper ocean hydrography (Bassinot et al., 1997; McIntyre and Molfino, 1996). Specifically, a decrease in abundance occurs when the nutricline is shallow, which is indicative of higher surface water nutrient content (e.g., McIntyre and Molfino, 1996).

Maxima in productivity agree well with minima in *Florisphaera* abundance (e.g., MIS 33, 26, 23, and 18). Cross-correlation between the two records confirms coherence above the 80% level near obliquity and at precession (Fig. 6a, b). Productivity maxima slightly lag *Florisphaera* minima (by 53° ± 23° at obliquity and by 44° ± 25° at precession, Fig. 6c). These results are consistent with increased productivity during times of higher surface water nutrient content, suggesting a top to bottom link between surface hydrography and benthic foraminiferal derived productivity on orbital time-scales.

3.4. South Atlantic ODP Site 1090

ODP Site 1090 (Fig. 2) lies at 3702 m water depth at the northern flank of the Agulhas Ridge in the southern Cape Basin at 41°S, just north of the Subantarctic Front (SAF) (Gersonde et al., 1999). Modern ocean productivity varies from 9 to 32 g C m^{-2}, with maxima during the austral summer months (Antoine et al., 1996; Table 1) when the SAF extends farthest north. The region is in a so-called high nitrate, low chlorophyll zone where external inputs of Fe can significantly affect primary productivity (e.g. Martin, 1990; Coale et al., 2004; Trick et al., 2017; Martinez-Garcia et al., 2009, 2011). It has been suggested that Fe inputs may have contributed to glacial to interglacial variations in the primary productivity of the region over the past four million years (Martinez-Garcia et al., 2011). These authors also observe that there is an increase in dust at this site during the MPT, pointing to the role of productivity changes in the evolution of the greater glaciation at this time.

Located near the mixing zone of lower NADW with circumpolar deep water, the stable isotope records (Fig. 7a and b) have provided much information on the orbital-scale evolution of Plio-Pleistocene

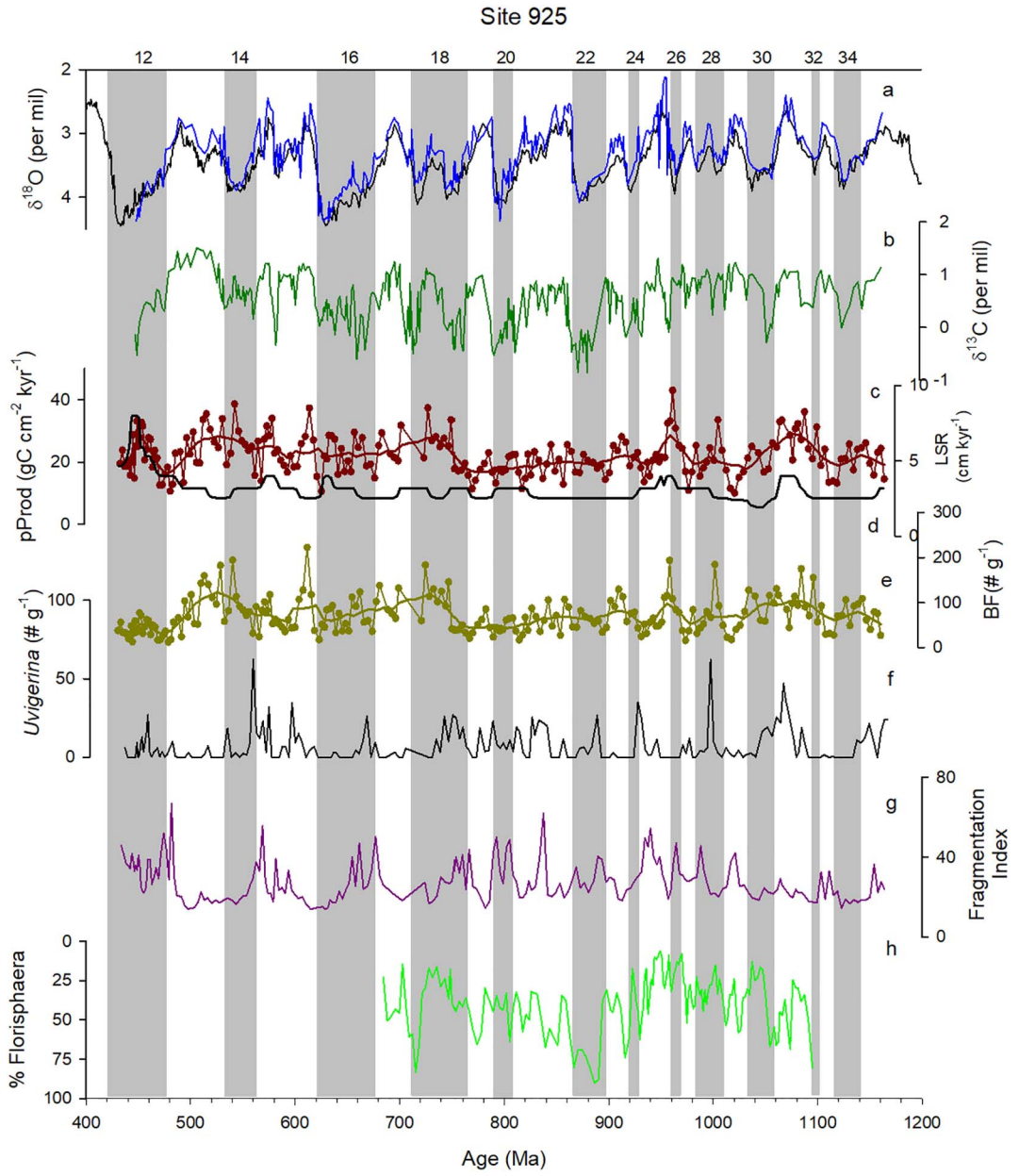

Fig. 5. Summary of results from tropical Atlantic Site 925. Benthic foraminiferal $\delta^{18}O$ (a) and $\delta^{13}C$ (b) (Bickert et al., 1997); Black line in panel (a) shows the global $\delta^{18}O$ stack of Lisiecki and Raymo (2005). Benthic foraminiferal-derived paleoproductivity (c), linear sedimentation rates (LSR) (d), benthic foraminiferal test counts per gram sediment (e), number of *Uvigerina* per gram sediment (f), fragmentation index (g); *Florisphaera* abundances (Beaufort et al., 2001) (h). Note that the y-axis in (h) is inverted to visually align *Florisphaera* minima with productivity maxima. Vertical grey boxes highlight the timing of glacial Marine Isotope Stages after Lisiecki and Raymo (2005).

deep water circulation and basin-wide carbon isotope gradients (e.g., Hodell and Venz-Curtis, 2006). Interestingly, the $\delta^{13}C$ minimum that distinguishes the mid-point of the MPT (MIS 22) at other sites is not as obvious at Site 1090 (Fig. 7b). A distinct and prolonged $\delta^{13}C$ minimum occurs for the first time 150 kyr earlier, during MIS 30.

Benthic foraminiferal-derived productivity increases during the earliest portion of the record, and a distinct maximum is reached during the MIS 30 interval of low $\delta^{13}C$ values (Fig. 7c). Thereafter productivity decreases with distinct minima during the early parts of interglacial MIS 25 and MIS 23. It does appear that the sedimentation rate multiplier (Fig. 7d) may have affected the productivity increase during the onset of the MPT because a unique trend toward higher values toward MIS 30 is not apparent in the benthic foraminiferal test counts (Fig. 7e). However, the maximum during MIS 30 is relatively robust, as are the minima during MIS 25 and 23.

With the exception of *Uvigerina*, whose abundance is low throughout (Fig. 7f), other records are consistent with productivity maxima during glacial and minima during interglacial times. Radiolaria display distinct maxima during glacial isotope stages (Fig. 7g), essentially paralleling the biogenic opal record (Diekmann and Kuhn, 2002, Fig. 7h). Fragmentation is highest during glacial intervals (Fig. 7i) as expected from enhanced respiration in the deep ocean in response to enhanced flux of organic matter and/or a decrease of the relative flux of northern-sourced deep waters. This may also indicate that the benthic foraminiferal counts might be biased by high fragmentation. The silica and fragmentation records display large similarities with Fe, sedimentary pyrite, and alkenone MARs (Fig. 7j, k, and l, respectively). In fact, there is an essentially one to one match between peaks in percent radiolaria, percent opal, Fe MARs, pyrite, and alkenone MARs during the glacial intervals. Agreement among the records is particularly pronounced during MIS 35 when all records exhibit minima with little variations across the entire interglacial interval.

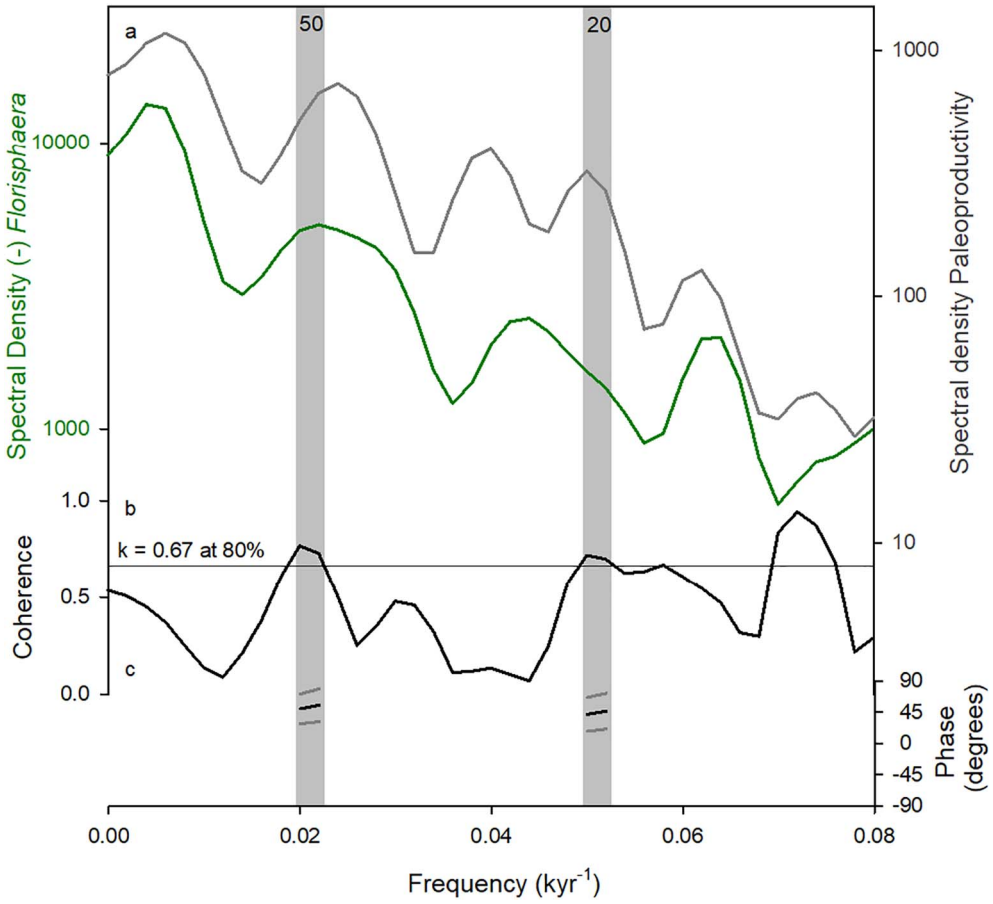

Fig. 6. Cross spectral analysis between Site 925 benthic foraminiferal-derived productivity and (−) % *Florisphaera* abundances (*Florisphaera* is multiplied by −1 in order to equate a shallow nutricline with high productivity) (a); coherence (b); and phase relationship (c). The two records are significantly (> 80%) correlated (at a periodicity of about 47 kyr) and in-phase suggesting that maximum benthic foraminiferal-derived productivity correlates with *Florisphaera* minima both indicative of increased nutrient content of surface waters.

Benthic foraminiferal-derived productivity variability remains relatively high and is not easily related to glacial-interglacial background conditions. As time series analysis illustrates, the data are coherent with $\delta^{18}O$ values at the 100 kyr cycle and precession (Table 2). Iterative analysis indicates that, as at Site 925, the significant coherence at the 100 kyr periodicity arises after the mid-point of the MPT (Table 3), but precession loses significance. When significant, the phase angles are rather large suggesting that productivity maxima are more closely related to glacial than interglacial intervals (Tables 2 and 3).

3.5. South Pacific ODP Site 1123

Site 1123 (171.5°W, 42°S, Fig. 2) is at 3290 m water depth on a sediment drift on the northeastern slopes of Chatham Rise (Carter et al., 1999). The site lies close to the southern reaches of the subtropical front, which separates micronutrient-rich (e.g., Fe) subtropical water from micronutrient-poor subantarctic waters (e.g., Lüer et al., 2008). Seasonal variations in productivity are relatively high (18–50 g C m^{-2}, Antoine et al., 1996; Table 1), with maxima during the austral spring and summer when subtropical water masses dominate.

As at the other sites, there is a close coupling between the benthic foraminiferal $\delta^{18}O$ and $\delta^{13}C$ records (Fig. 8a and b, respectively). Supported by variations in the sortable silt fraction of the sediments, the record reflects variations in the strength of the Deep Western Boundary Current reaching the site on glacial to interglacial time scales (Hall et al., 2001). The $\delta^{13}C$ minimum associated with the mid-point of the MPT (MIS 24-22) is pronounced and reflects, at least in part, reduced proportion of NADW in the Pacific sector of the Southern Ocean (Elderfield et al., 2012), which is consistent with the emerging picture of a reduced rate of deep water circulation at the time (Schmieder et al., 2000; Pena and Goldstein, 2014).

At Site 1123, benthic foraminiferal-derived productivity does not display a long-term trend during the onset of the MPT (Fig. 8c). It does, however, show a drastic decrease in the amplitude of variability following the mid-point of the transition (MIS 22/21). The pattern is also apparent in the benthic foraminiferal counts (Fig. 8e), and it is clearly not a function of the sedimentation rate multiplier (Fig. 8d).

Other faunal derived proxies are also dominated by glacial to interglacial-scale variations. The pattern is not so clear in *Uvigerina*, however, which displays a distinct maximum during glacial MIS 22 but also during interglacial MIS 35 and 15 (Fig. 8f). Radiolarian abundances, on the other hand, increase more consistently during glacial intervals, with distinct maxima during MIS 24 and MIS 22 (Fig. 8g). Foraminiferal fragmentation also tends to be higher during glacial intervals (Fig. 8h). The record is thus largely similar to the radiolaria with increased fragmentation, and hence dissolution, when radiolarian abundances are relatively high (Fig. 8g), consistent with top-to-bottom organic matter transfer. In this vein, we cannot rule out that the absolute magnitude of benthic foraminiferal-derived productivity is not enhanced by planktic foraminiferal test dissolution. The abundance of pyrite particles is relatively constant throughout, with the notable exception of a first distinct peak during glacial MIS 24 followed by others that do not appear to be related to glacial/interglacial background conditions (Fig. 8i).

Time series analysis illustrates that the overall variability in productivity is related to orbital forcing (Table 2). As at Sites 925 and 1090, the 100 kyr cycle becomes significant after the mid-point of the MPT (Table 3). Coherence in the obliquity and precession bands is also significant, but only prior to the mid-point of the MPT (Table 3). In all three bands, the phase angles are larger than a quarter cycle suggesting that the productivity maxima are more closely related in timing to glacial then interglacial intervals.

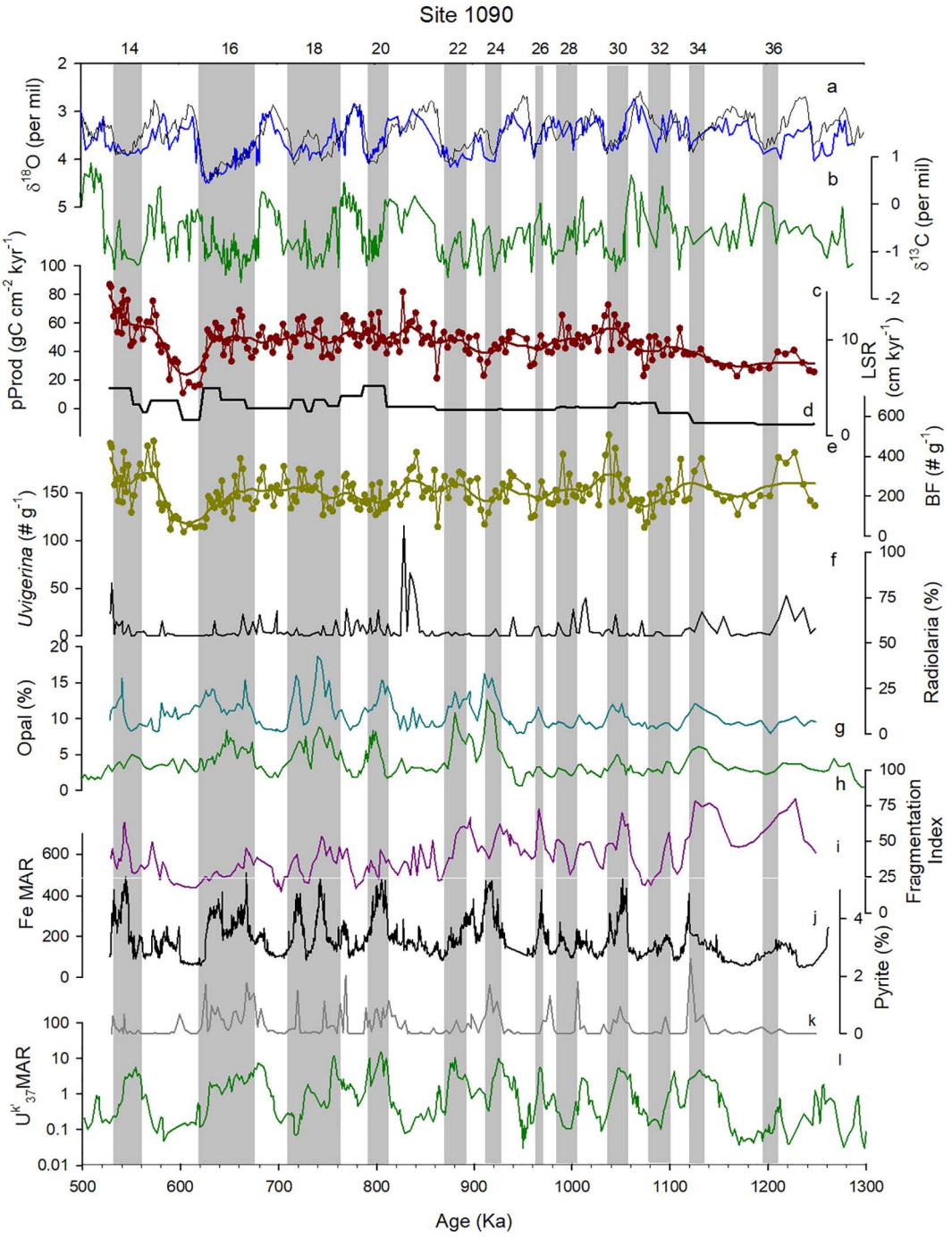

Fig. 7. Summary of results from South Atlantic Site 1090. Benthic foraminiferal $\delta^{18}O$ (a) and $\delta^{13}C$ (b) (Martinez-Garcia et al., 2011). Black line in panel (a) shows the global $\delta^{18}O$ stack of Lisiecki and Raymo (2005). Benthic foraminiferal-derived paleoproductivity (c), linear sedimentation rates (LSR) (d), benthic foraminiferal test counts per gram sediment (e), number of *Uvigerina* per gram sediment (f), percent radiolaria (g), percent biogenic silica (opal) (Diekmann and Kuhn, 2002) (h); fragmentation index (see text) (i); XRF-derived Fe mass accumulation rates (Martinez-Garcia et al., 2010) (j), percent sedimentary pyrite (k); alkenone mass accumulation rates ($U^{k'}_{37}$ index) (Martinez-Garcia et al., 2011) (l). Vertical grey boxes highlight the timing of glacial Marine Isotope Stages after Lisiecki and Raymo (2005).

3.6. Eastern equatorial Pacific Ocean ODP Site 849

ODP Site 849 is on the western flank of the East Pacific Rise in the eastern equatorial Pacific (Mayer et al., 1992) (Fig. 2). At 0°11′N, 110°W, Site 849 lies within the eastern equatorial Pacific cold tongue (Martinez-Garcia et al., 2010), which is the equatorial divergence zone where upwelling of cold, nutrient rich waters from below the thermocline characterize upper ocean hydrography. Modern day seasonal productivity varies between 27–50 g C m^{-2} (Antoine et al., 1996; Table 1).

At 3851 m water depth, the stable isotope records from Site 849 reflect the glacial to interglacial variations in whole ocean $\delta^{13}C$ values (Mix et al., 1995). The tight coupling between $\delta^{18}O$ and $\delta^{13}C$ values (Fig. 9a and b, respectively) is commonly interpreted to reflect transfer of carbon between the terrestrial and marine reservoirs. The presence of a pronounced $\delta^{13}C$ minimum during the mid-point of the MPT indicates that this feature is, at least in part, associated with such global and terrestrial-linked processes rather than solely due to processes associated with deep water circulation.

A gradual increase in benthic foraminiferal productivity maxima

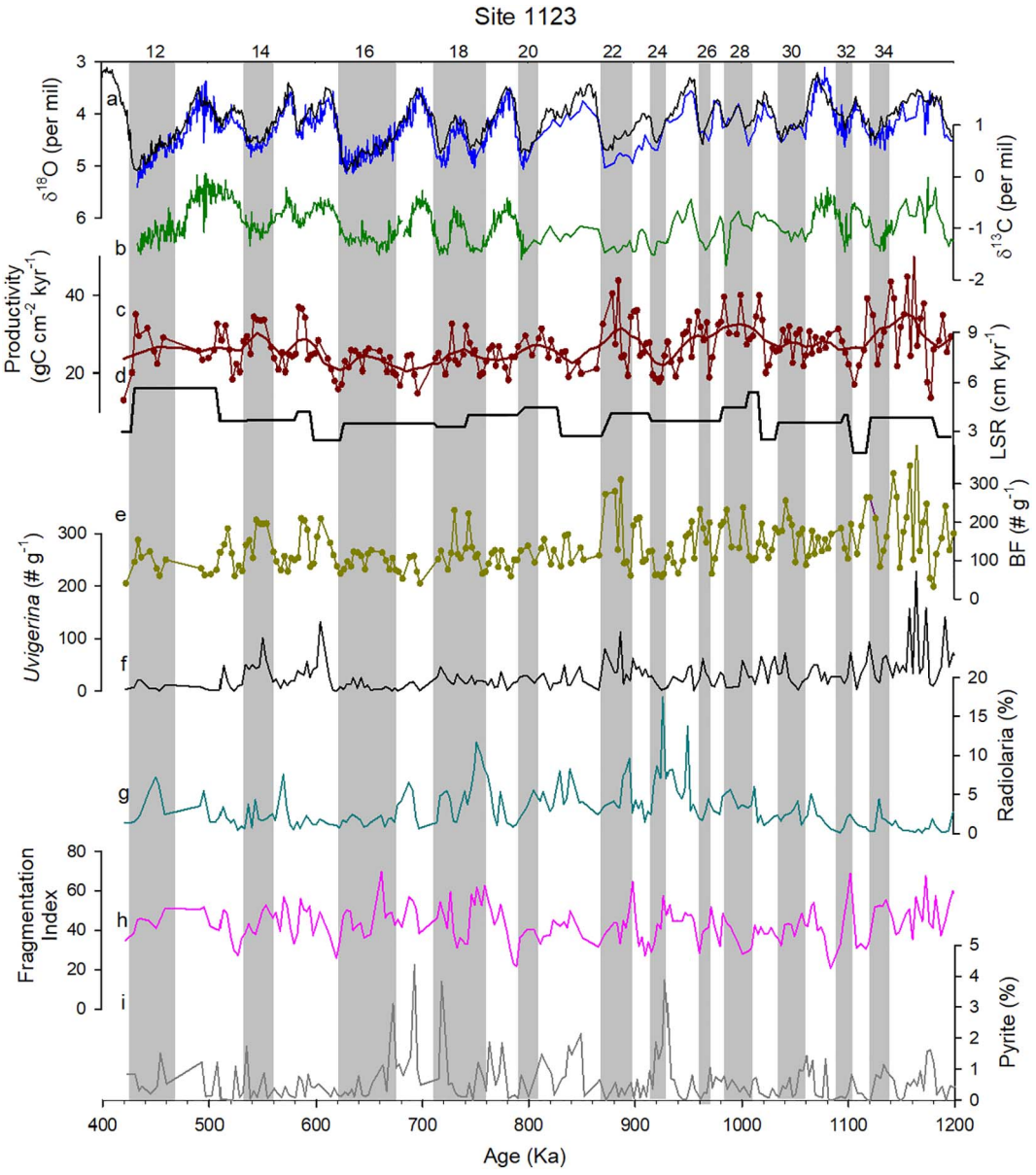

Fig. 8. Summary of results from southwestern Pacific Site 1123. Benthic foraminiferal $\delta^{18}O$ (a) and $\delta^{13}C$ (b) (Hall et al., 2001; Elderfield et al., 2012). Black line in panel (a) shows the global $\delta^{18}O$ stack of Lisiecki and Raymo (2005). Benthic foraminiferal-derived paleoproductivity (c), linear sedimentation rates (LSR) (d), benthic foraminiferal test counts per gram sediment (e), number of *Uvigerina* per gram sediment (f), percent radiolaria (g), fragmentation index (see text) (h), and percent sedimentary pyrite (i). Vertical grey boxes highlight the timing of glacial Marine Isotope Stages after Lisiecki and Raymo (2005).

occurs during the onset of the MPT with a distinct maximum during interglacial MIS 21. The trend and maximum are also apparent in the foraminiferal counts (Fig. 9e). Productivity maxima are primarily associated with interglacial intervals (Fig. 9c). Although the absolute magnitude of the maxima is likely affected by the sedimentation rate multiplier (Fig. 9d), the variations are robust as they are apparent in the original benthic foraminiferal test counts.

Primarily interglacial productivity maxima are evidenced by *Uvigerina* (Fig. 9f) and radiolaria (Fig. 9g) maxima. Large diatom (> 63 μm) abundance comes to a pronounced maximum during MIS 21, but drops to essentially zero thereafter (a minor increase occurs during MIS 17, Fig. 9h). The number of fragments in the Site 849 sediments is relatively high throughout, and distinct maxima occur primarily during interglacial intervals (Fig. 9i). At this site, there is good agreement among proxy records that is consistent with a top to bottom link of primary production in the upper water column and degradation of organic matter in the deep ocean.

However, prior work in the region (e.g., Farrell and Prell, 1999; Sexton and Barker, 2012) and the high degree of foraminiferal test fragmentation (> 50% suggest carbonate dissolution is particularly high during interglacial intervals. Therefore, we cannot rule out that enhanced carbonate dissolution may have artificially increased the number of more dissolution-resistant benthic foraminiferal tests (including *Uvigerina*) and other faunal components such as the radiolaria and diatoms in the samples. The effect may have biased reconstructions of absolute values of productivity, but the general trends are likely robust.

Time series analysis supports that productivity maxima are significantly correlated with $\delta^{18}O$ values only at obliquity and precessional periodicities; there is no coherence at the 100 kyr periodicity (Table 2). In the obliquity band, productivity lags interglacial conditions by roughly one quarter cycle, and, within error, the phase relationships do not change across the MPT. At precession, the phase angles are also constant within error, but larger than a quarter cycle

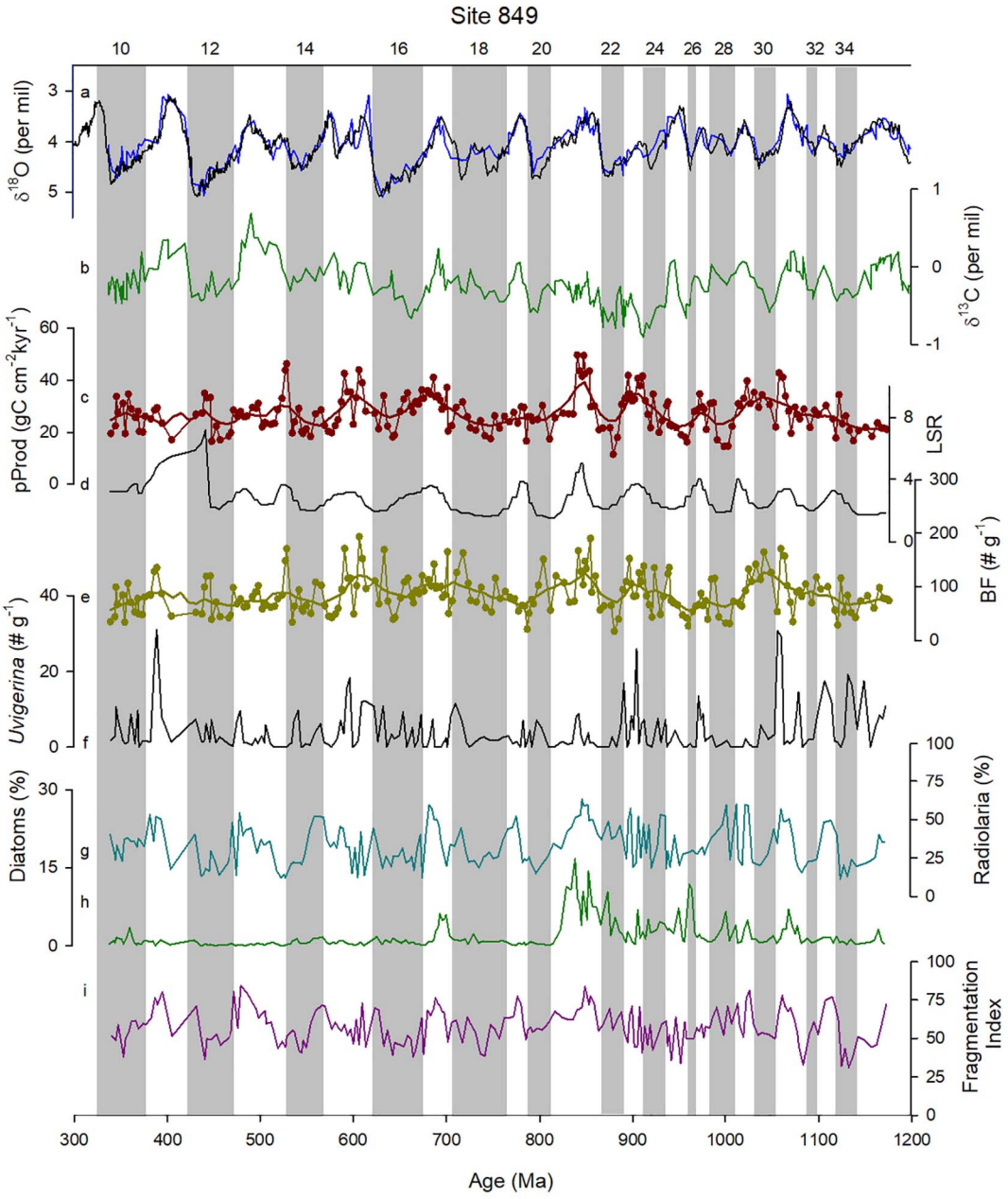

Fig. 9. Summary of results from eastern equatorial Pacific Site 849. Benthic foraminiferal $\delta^{18}O$ (a) and $\delta^{13}C$ (b) (Mix et al., 1995); Black line in panel (a) shows the global $\delta^{18}O$ stack of Lisiecki and Raymo (2005). Benthic foraminiferal-derived paleoproductivity (c), linear sedimentation rates (LSR) (d), benthic foraminiferal test counts per gram sediment (e), number of *Uvigerina* per gram sediment (f), percent radiolaria (g), percent large diatoms (g), fragmentation index (see text) (h). The solid grey line in (a) reflect that benthic foraminiferal $\delta^{18}O$ stack of Lisiecki and Raymo (2005). Vertical grey boxes highlight the timing of glacial Marine Isotope Stages after Lisiecki and Raymo (2005).

suggesting that productivity is more closely related to glacial conditions (Table 3).

3.7. Western equatorial Pacific ODP Site 806

Site 806 (0°N, 159°E, Fig. 2) is at 2532 m water depth on the Ontong Java Plateau in the western equatorial Pacific (Kroenke et al., 1991). The location of Site 806 in the western equatorial Pacific warm pool implies weak seasonal hydrographic variability with a deep thermocline (> 100 m). Accordingly, productivity remains relative low throughout the year (18–32 g C m^{-2} season^{-1}; Antoine et al., 1996; Table 1).

As at Site 849, benthic foraminiferal $\delta^{18}O$ and $\delta^{13}C$ values are strongly coupled, reflecting global variations in climate and the $\delta^{13}C$ value of Pacific deep water (Bickert et al., 1993, Bickert, pers. communication, 2016) (Fig. 10a and b, respectively). The $\delta^{13}C$ minimum defining the mid-point of the MPT (MIS 24-22) is pronounced, and, as at Site 849, it underscores the global nature of this phenomenon.

As at Site 849, benthic foraminiferal-derived productivity increases during the onset of the MPT with a distinct maximum during the mid-point interglacial MIS 21 (Fig. 10c). LSR show a similar trend (Fig. 10d) and can explain all but the maximum during MIS 21. Benthic foraminiferal test counts would support an overall increase in productivity during the onset of the MPT and the distinct maximum during its mid-point (MIS 21) (Fig. 10e). However, it is not clear to what extent the long-term trend is unique; it may be part of a recurrent pattern that begins with a decrease in productivity between MIS 35 and 34. *Uvigerina* abundance is relatively high at this site, and it, too, after an initial decrease, displays a longer-term increase toward the mid-point of

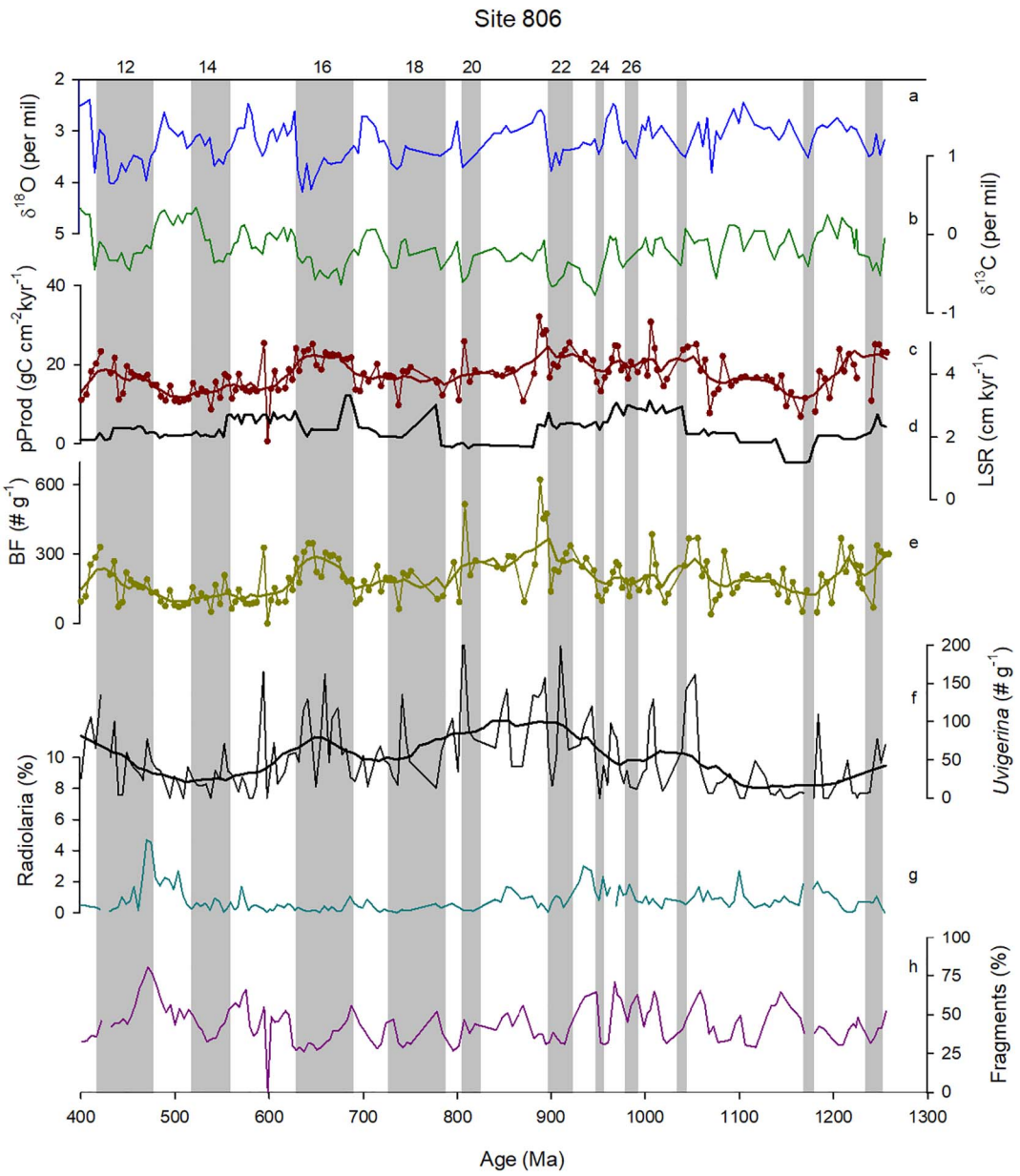

Fig. 10. Summary of results from eastern equatorial Pacific Site 806: Benthic foraminiferal $\delta^{18}O$ (a) and $\delta^{13}C$ (b) (Karas et al., 2009); Benthic foraminiferal-derived paleoproductivity (c), linear sedimentation rates (LSR) (d), benthic foraminiferal test counts per gram sediment (e), number of *Uvigerina* per gram sediment (f), percent radiolaria (g), fragmentation index (see text) (h). Vertical grey boxes identify the timing of maxima in the Site 806 benthic foraminiferal $\delta^{18}O$ record. Only those that we can confidently assign to glacial MIS stages are labeled.

the MPT (Fig. 10f). Radiolaria are rare but do display some increase toward MIS 23 (Fig. 10g). The fragmentation index does not show any long-term trend, but the abundance of fragments is relatively low during the initial stages of MIS 21 (Fig. 10h) and are thus not artificially enhancing the MIS 21 maximum in benthic foraminiferal tests.

As at Site 849, productivity maxima tend to occur during interglacial intervals, at least until MIS 21. Thereafter, it appears that productivity maxima occur primarily during glacial intervals such as MIS 16 and 12. This pattern is reflected in the benthic foraminiferal data (Fig. 10c and e) including the *Uvigerina* counts (Fig. 10f).

4. Discussion of productivity in a regional context

4.1. Subpolar North Atlantic Site 552

In the subpolar North Atlantic, there is some evidence for increased productivity during the onset of the MPT between MIS 30-28. This interpretation is supported by productivity reconstructions based on benthic foraminiferal counts, radiolaria, as well as the production of organic matter as evidenced by alkenone MARs in this region. As productivity maxima occur during glacial as well as interglacial intervals, they cannot easily be ascribed to consistent changes in hydrography. During the mid-point of the MPT, as best expressed by the alkenone MARs, productivity is low but terrigenous inputs are high, particularly during the two glacial intervals, MIS 24 and 22. This observation agrees with data from more northern and western Site U1314, which show high glacial inputs of IRD, but low opal fluxes and radiolarian diversity at this time (Hernandez-Almeida et al., 2013). In fact, maximum terrigenous input during glacial maxima, or at the transition from glacial to interglacial phases (Diester-Haass and Schnitker, 1989; Hernandez-Almeida et al., 2013) is typical for sites in this latitude belt (e.g., Marino et al., 2011; Alonso-Garcia et al., 2011; Hernandez-Almeida et al., 2013) and likely reflects a southward shift of the polar front as ice sheets extended toward Pleistocene maxima (e.g., McClymont et al.,

2008; Alonso-Garcia et al., 2011; Knies et al., 2009; Marino et al., 2011). As Site 552 lies farther south than those sites used in previous reconstructions, our data indicate an even more southern position of the Arctic Front than previously shown. Decreasing, and/or minimal productivity at MIS 24-22 might reflect enhanced stratification of the upper ocean due to cooling and/or meltwater reducing biological productivity (Ruddiman and McIntyre, 1981; Diester-Haass and Schnitker, 1989; Hernandez-Almeida et al., 2013). We speculate that these hydrographic changes may have dampened the relative amount of deep water forming in the North Atlantic and thereby contributed to the thermohaline circulation 'crisis' characterizing the mid-point of the MPT (Pena and Goldstein, 2014).

4.2. North Atlantic Site 607

At this site, long-term trends in productivity are equivocal. Benthic foraminiferal tests indicate some increase in productivity during the onset of the MPT in the North Atlantic Ocean toward MIS 28, but alkenone MARs do not support it. Alkenone MARs indicate a maximum during the mid-point but no long-term trend prior. Benthic foraminiferal trace metal ratios (Cd/Ca and B/Ca) at Site 607 provide evidence for an increase in deep water nutrient content during the onset of the MPT, culminating in a maximum during the mid-point; however, the data also demonstrate that deep water nutrients are associated with variations in the relative flux of bottom water masses rather than with overlying primary productivity (Lear et al., 2016).

On glacial to interglacial time-scales, the proxy records are more consistent with changes in ocean atmosphere interactions than with external nutrient inputs. Maxima in radiolaria and alkenone MARs during glacial intervals likely reflect enhanced upwelling of nutrient-rich deep waters as the subtropical gyre and the axis of westerly winds move above the study site (Lawrence et al., 2013). The generally low IRD counts reflect that only few icebergs drifted this far south even during the glacial extremes, consistent with the site's position south of the polar front even during the Last Glacial Maximum (Stein et al., 2009). The presence of IRD, however, would be consistent with cooling of North Atlantic sea surface temperatures at this time (Ruddiman et al., 1986). Accordingly, the gradual increase in IRD during the onset of the MPT may reflect the adjustment of the Arctic Front to the expansion of NH glaciers. Glacial Fe/Ca peaks may relate to generally increased continental aridity consistent with enhanced glacial dust inputs beginning in the early Pleistocene (Lang et al., 2014) and the site's position more effectively underneath the westerly winds during those intervals (Naafs et al., 2010; Naafs et al., 2012). Interglacial Fe/Ca maxima may reflect a more meridional component of atmospheric circulation allowing the northward transport of Saharan dust into the mid latitudes of the North Atlantic Ocean (Stein et al., 2009).

4.3. Northwestern tropical Atlantic Ocean Site 925

At Site 925, there are no longer-term trends that would support an enhanced biological pump during the onset of the MPT. Rather, the records are dominated by orbital-scale variations that most likely reflect a regional hydrographic response to orbital forcing. As the time series analysis indicates, coherence at the 100 kyr cycle becomes significant after the mid-point of the MPT, which is consistent with the fact that benthic foraminiferal $\delta^{18}O$ records do not contain power at this periodicity prior to this time. The relatively long phase angle indicates that productivity maxima occur more closely related to glacial than interglacial intervals. This particular aspect would be consistent with a link between primary productivity and climate change. In the obliquity and precession bands, however, the phasing changes. Before the mid-point of the MPT, both bands exhibit large phase angles indicating that productivity maxima occur closer in timing to glacial than to interglacial maxima. After the mid-point, however, the phase angles in both bands are smaller, less than a quarter cycle, suggesting a closer association with interglacial conditions. Thus, there is no consistent timing between glacial to interglacial climate change and productivity that would evidence a role for primary productivity as a driver for MPT climate change.

The comparison with nannofossil *Florisphaera* demonstrates that benthic foraminiferal-derived productivity variations are an environmental response to changes in upper ocean hydrography. The analysis also demonstrates a close top-to-bottom link between surface hydrography and deep ocean organic carbon flux on orbital time-scales. At this site, variations in the nutrient content of the upper ocean depend on thermocline depth, which is regulated by trade wind strength and the meridional position of the ITCZ (Bassinot et al., 1997). In this vein, the change in the nature of the productivity-$\delta^{18}O$ phase relationships during the MPT could also signal a regional change in the response of the upper ocean to orbital forcing. A close, albeit anti-phased, tie between the surface and deep was observed in previous study from this region linking nannofossil Sr/Ca ratios with benthic foraminiferal accumulation rates during the middle Pliocene (Waite et al., 2008). While the comparison illustrates a proof of concept for what is to be expected based on our understanding of the modern ocean, it does not provide evidence for a driving role of the biological pump in the climatic changes related to the MPT.

4.4. South Atlantic Site 1090

As in the western tropical Atlantic, benthic foraminiferal-derived productivity at Site 1090 does not unambiguously support a role for the biological pump during the onset of the MPT. The apparent long-term increase in productivity may have been introduced by the sedimentation rate multiplier. As at Site 925, a link between benthic foraminiferal-derived productivity and climate becomes significant with the evolution of the 100 kyr climate cycle.

Orbital-scale changes in productivity linked to the 100 kyr climate cycle are well documented in the published silica and Fe and alkenone MAR records at Site 1090 (Diekmann and Kuhn, 2002; Becquey and Gersonde, 2002, Martinez-Garcia et al., 2011). As is typical for sites located in the subantarctic zone north of the polar front, opal deposition increases during glacial intervals due to the advection of silica-rich surface water from the south as the frontal zones expand to the north (e.g., Charles et al., 1991; Diekmann and Kuhn, 2002, Fig. 7h). Increases in silica productivity are tightly coupled to enhanced dust flux, which bears bioavailable Fe (Martinez-Garcia et al., 2011, e.g., Fig. 7j). Not only biogenic silica but also carbonate productivity increased during glacial intervals, as indicated by alkenone MARs (Martinez-Garcia et al., 2011, Fig. 7l). Thus, the benthic foraminiferal data provide independent support of interpretations of previously published productivity proxies that suggest an enhanced biological pump during glacial intervals perhaps associated with equatorward migration of the polar and subpolar frontal zones and/or increased Fe fluxes (Diekmann and Kuhn, 2002; Martinez-Garcia et al., 2011).

Our new pyrite data provide direct evidence in support of a stagnant deep South Atlantic during the more prominent glacial intervals of the MPT (MIS 34, 30, 24, 20, 18, 16) (Fig. 7k). Pyritization requires large amount of organic matter to create suboxic conditions as well as an Fe source (e.g., Berner, 1984), eolian in this case (Diekmann and Kuhn, 2002; Martinez-Garcia et al., 2011). Both conditions are met as evidenced by distinct peaks in opal, radiolarian, alkenone, and Fe content of the sediments at these times. Low oxygen conditions could be maintained also by a reduction in the relative rate of ventilated bottom waters associated with a more sluggish deep water circulation during glacial intervals (Venz and Hodell, 2002; Hodell and Venz-Curtis, 2006). The distinct pyrite peak during MIS 24, in particular, is consistent with weakened thermohaline circulation during the mid-point of the MPT (Schmieder et al., 2000; Poirier and Billups, 2014; Pena and Goldstein, 2014).

4.5. South Pacific Site 1123

No evidence exists as Site 1123 for a long-term increase in productivity at this site to support an increase in the biological pump as a mechanism playing a role in the onset of the MPT. An abrupt decrease occurs in the amplitude of the variability of the benthic foraminiferal time series during the mid-point of the MPT (~900 ka), an observation that does not characterize the other proxies. In fact, while MIS 35 is an interval of quiescence at Site 1090, at Site 1123, high amplitude productivity variations persist, an observation consistent with sea surface temperature reconstructions across this interval of time (Crundwell et al., 2008). Differences between these two Southern Ocean sites are likely related to the position of each site with respect to the regional meridional movements of the subpolar and subtropical frontal zones and associated surface current system. During MIS 35, Site 1090 appears to have remained north of the subpolar frontal zone, while the location of Site 1123 was highly sensitive to meridional movements of subtropical versus subantarctic surface waters (e.g., Crundwell et al., 2008).

However, as at the other sites, we observe an association of enhanced productivity with glacial intervals at the 100 kyr cycle providing evidence for a link between the biological pump and climate change. At Site 1123, iterative cross-spectral analysis illustrates obliquity and precession-scale productivity and $\delta^{18}O$ correlations are also significant before 800 Ka and are also related to glacial climates.

Similar to Site 1090, during the mid-point glacial interval of the MPT (MIS 24), there is a distinct maximum in pyrite. As at Site 1090, the pyrite peak corresponds with a maximum in radiolarian abundance. Although there is no direct Fe record at Site 1123, the amount of externally supplied Fe reaching the site may have increased during glacial intervals as evidenced by generally enhanced Fe fluxes at other South Pacific sites (Hesse, 1994; Lamy et al., 2014). Thus, it appears that the mid-point of the MPT was accompanied by increased primary productivity and carbon export to the deep ocean and into the sediments. In this vein, and further evidenced by particularly low benthic foraminiferal $\delta^{13}C$ values during MIS 24, low oxygen conditions are consistent with a more sluggish ventilation of the bottom waters due to a reduction in the rate of deep water circulation. Taken in context with similar results from Site 1090 during this general interval of time, these observations provide evidence for the extra regional nature of this phenomenon and strengthen interpretations of a sluggish thermohaline circulation during the mid-point of the MPT.

4.6. Eastern equatorial Pacific Site 849

Site 849 displays a trend toward higher productivity during the onset of the MPT culminating in a distinct maximum during its mid-point (MIS 21). These results are largely consistent with barium MARs from this site that show an increase beginning at around 1 Ma (Ma et al., 2015). However, barium MARs continue to increase toward the late Pleistocene while benthic foraminiferal-derived productivity continues to fluctuate.

On the obliquity-scale, productivity appears to be higher during interglacial than glacial intervals, and these relationships do not change across the MPT (e.g., Table 3). These results are similar to barium accumulation rates at the same site (Ma et al., 2015), lending support to the importance of upper ocean hydrographic changes on the primary productivity of the site on glacial to interglacial time scales. Located at the western end of the present day eastern equatorial Pacific cold tongue, the upper waters receive micro and macro nutrients from Subantarctic Mode water (Toggweiler et al., 1991; Sarmiento et al., 2004). As previously discussed by Lawrence et al. (2013) and Ma et al. (2015), lower glacial than interglacial productivity in this region appears to mirror higher glacial and lower interglacial productivity in the source region for the thermocline waters, the southeast Pacific intermediate water. We note that in the obliquity band, the phasing at Site 849 is opposite of the phasing at Site 1123 for this interval of time. Such an anti-phased relationship between Site 849 and 1123 is also apparent in the time series during mid-point MIS 22 and MIS 21 when a distinct productivity minimum at Site 849 corresponds to a distinct maximum at Site 1123 for the former, and a distinct maximum at Site 849 corresponds to a distinct minimum at Site 1123 during the latter (e.g., Figs. 8c and 9c). These observations support a high to low latitude nutrient link, which has been implicated in other studies (e.g., Lyle et al., 1992; Liu and Herbert, 2004; Lawrence et al., 2013; Ma et al., 2015).

4.7. Western equatorial Pacific Site 806

The longer-term increase in interglacial productivity during the onset of the MPT as well as generally interglacial productivity maxima until its mid-point, may reflect processes similar to those in the eastern equatorial Pacific (Site 849). Higher productivity during individual interglacial intervals may thus be related to higher nutrient content in the high latitude source waters, which are then advected westward. The observation suggests coherent productivity variations across the equatorial Pacific, which have been observed during the Pliocene and ascribed to variations in nutrient content via high latitude forcing (Bolton et al., 2010).

At Site 806, productivity appears to display maxima during glacial intervals after the mid-point of the MPT. This observation is consistent with late Quaternary productivity reconstructions (Bickert et al., 1993; Yasuda et al., 1993; Rea et al., 1991; Paytan et al., 1996; Beaufort et al., 2001; Murray et al., 2012). Glacial productivity is ascribed to a larger zonal temperature gradient during glacial periods (Lea et al., 2000) and stronger wind activity and Walker circulation (Rea et al., 1991; Winckler et al., 2008; Murray et al., 2012; Xu et al., 2015). Thus, at Site 806, the mid-point of the MPT marks a fundamental change in response from high to low latitude forcing. Our records therefore suggest that, in the equatorial warm pool at least, the shift in climate state across the MPT impacted the response of low latitude productivity to orbital forcing.

5. Synthesis

Most of the sites investigated in this study display some degree of increasing benthic foraminiferal-derived productivity sometime during the onset of the MPT (Sites 552, 607, 925, 1090, 849, and 806, Fig. 11). However, the onset and duration of the productivity increases are not the same at each site. Furthermore, there is evidence that the magnitude of the site-specific productivity increase may be affected by the sedimentation rate multiplier (Sites 552, 1090, 806), the degree of dilution by other sediment constituents (Site 552), or that they are part of a longer-term, quasi-cyclical pattern (Sites 607, 1090, 849, and 806). These observations complicate the interpretation of the absolute magnitude of the reconstructed productivity increases. Because the majority of the sites display an increase in productivity during the onset of the MPT, the biological pump may have played a role in the transfer of CO_2 from the atmosphere into the deep ocean. However, the role of the biological pump as a driving mechanism for climatic cooling during the onset of the MPT is not evident in the data sets.

Neither are there global-scale coherent productivity trends during the mid-point of the MPT (MIS 24-20, 930–870 ka) (Fig. 11). In fact, productivity tends to be lower during this interval of time than before or after. Site 1123 in the South Pacific and Sites 806 and 849 in the equatorial Pacific are the only sites that show any type of maximum in productivity at this time (Fig. 11e, f, and g, respectively). Sites 849 and 1123, specifically, show an anti-phased relationship during mid-points of MIS 22 and 21. Although these results underscore the importance of a high to low latitude link, they do not support a link between productivity and climate change during the MPT.

Individual sites follow different glacial to interglacial patterns, and

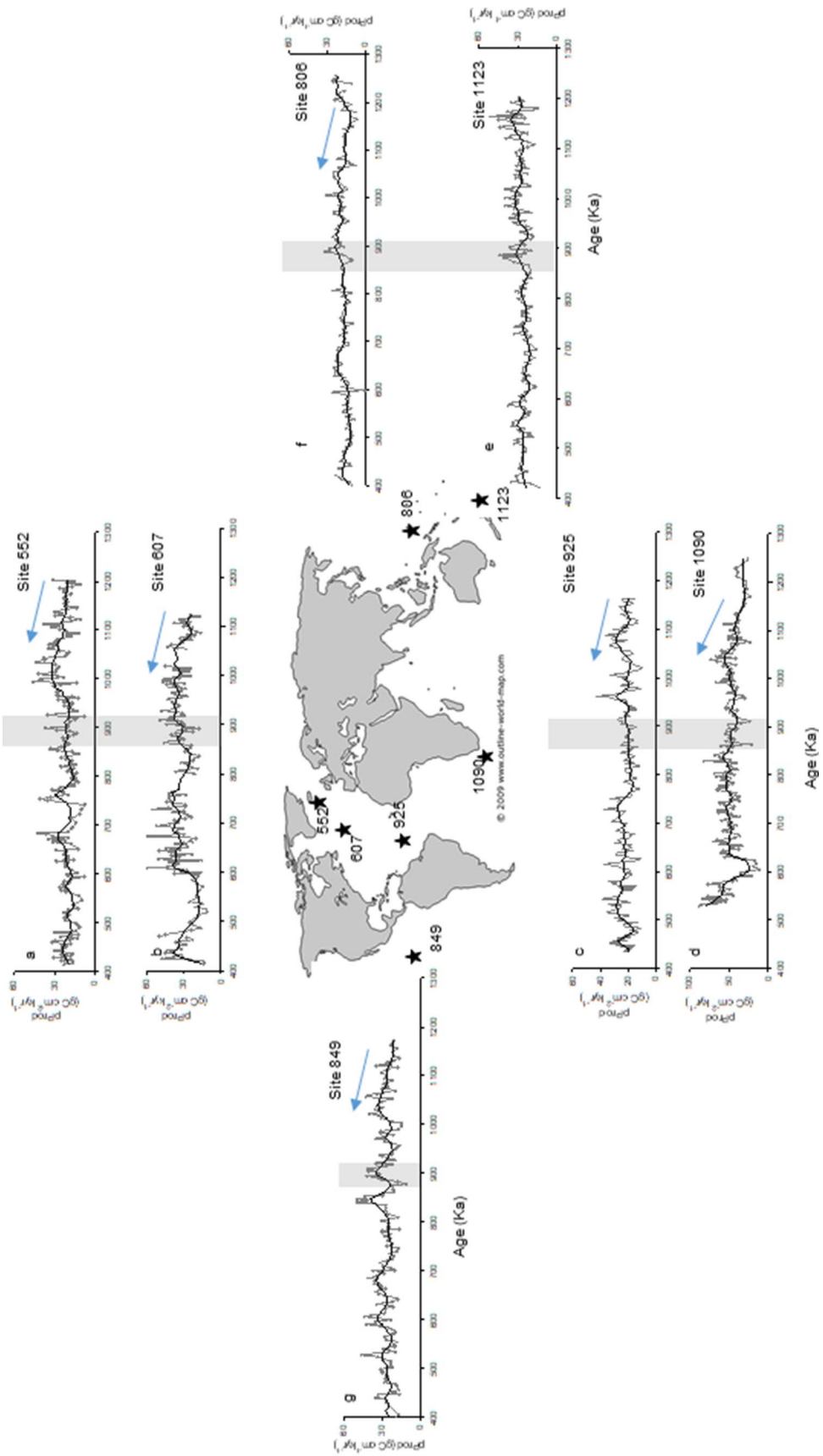

Fig. 11. Synthesis of benthic foraminiferal-derived paleoproductivity records in the context of this study. Grey bar highlights the mid-point of the mid-Pleistocene transition (MPT) between about 930–870 ka (Marine Isotope Stages 24-22). Light blue arrow is to demark the increase in paleoproductivity apparent in the records during the onset of the MPT.

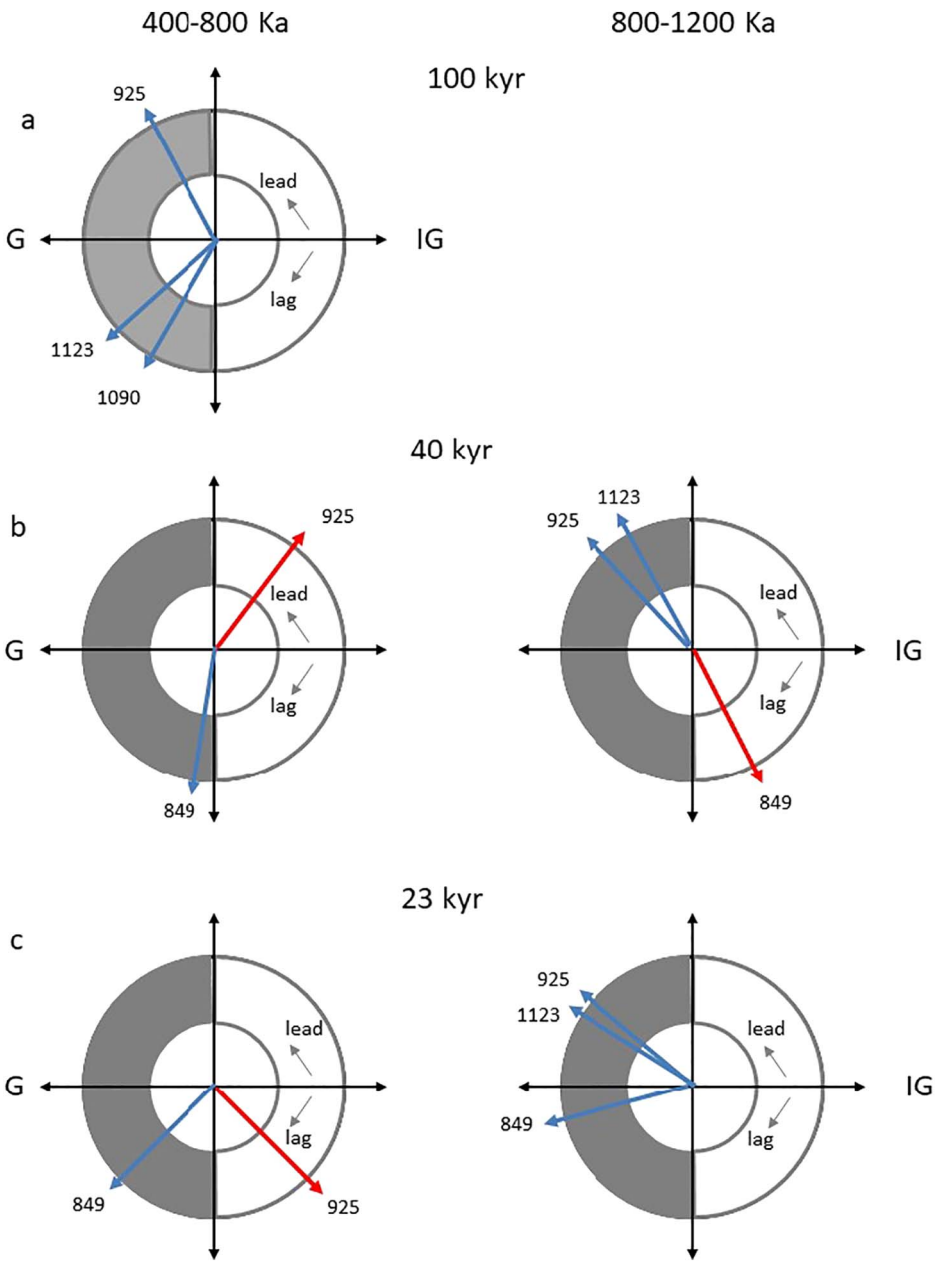

Fig. 12. Synthesis of significant phase relationships between (−) $\delta^{18}O$ records and benthic foraminiferal-derived productivity. Interglacial maxima correspond to a On each phase wheel, reference is with respect to interglacial (IG) maxima at the origin of the circle (0°). Glacial (G) maxima are at 180°. Negative phase angles, indicating that productivity leads interglacial maxima, are denoted by arrows in a counterclockwise fashion. Positive phase angles indicating that productivity lags interglacial maxima, are denoted by arrows in a clockwise fashion. Grey shaded portion highlight glacial maxima plus/minus one quarter cycle.

the nature of the temporal relationships differ among the orbital bands (Table 3, Fig. 12). At three sites (925, 1090, 1123), a significant relationship arises at the 100 kyr cycle after the mid-point of the MPT, and in each case productivity maxima are more closely associated in time with glacial than interglacial conditions (Fig. 12a). Correlation and phasing during the younger time slice is consistent with a larger driving force on the biological pump imparted by the growth and decay of large Northern Hemisphere glaciers.

The response in the obliquity and precession bands is less consistent overall (Fig. 12b, and c, respectively. High productivity tends to occur more closely related to glacial than interglacial intervals prior to the mid-point of the MPT. This relation is evident not only in the Southern Ocean (Site 1123), but also in the tropical Atlantic (Site 925) and, at precession intervals only, the eastern equatorial Pacific (Site 849). High interglacial productivity, on the other hand, is evident in both orbital bands at tropical Site 925 after the mid-point of the MPT. In the obliquity band, high interglacial productivity characterizes eastern equatorial Pacific Site 849 through the entire MPT. In short, these observations highlight that at obliquity and precession, there is no overall control on productivity response at the individual sites highlighting the importance of regional controls on productivity.

Although our data sets do not deliver unequivocal evidence regarding global productivity changes during the MPT, we highlight that the two Southern Ocean sites provide supporting evidence for a sluggish thermohaline circulation during its mid-point. Significant reduction in northern-sourced deep waters into the South Atlantic (Site 1090) during MIS 24-22 is reflected in a distinct maximum in neodymium isotope records (Pena and Goldstein, 2014). Trace metal ratios indicate a lowering of the carbonate saturation state between MIS 24 and 22 in support of enhanced glacial deep ocean carbon storage (Lear et al.,

2016). In our data set glacial MIS 24 stands out with a distinct maximum in pyrite at both Southern Ocean sites, which can be explained by sluggish deep water circulation lowering the oxygen content of bottom waters when Fe content and overlying surface water productivity are high.

6. Conclusion

Although the majority of our sites display an increase in productivity at the beginning of the MPT, our records do not provide strong support for the initial hypothesis that the mid-Pleistocene climate evolution is linked to widespread biologically mediated draw-down of CO_2. The data are thus consistent with the available CO_2 reconstructions that do not indicate a marked long-term decrease in CO_2 across this interval of time. As evidenced by three of our sites, the more intense, 100 kyr-paced glaciations following the MPT, however, can be linked to productivity and thus potentially to reduced pCO_2 as more carbon was stored in deep waters. The lack of more consistent variation in the productivity records between our seven selected sites highlights the numerous complex controls on this important feedback in the climate system.

Our records contribute to the emerging picture of the mid-point of the MPT, MI 24-22, as a critical time interval for global changes in deep water circulation. In the subarctic North Atlantic, the source region for Northern Hemisphere deep water masses, reduced productivity and enhanced IRD inputs are consistent with enhanced stratification and reduced North Atlantic Deep Water production during this interval of time. In the South Atlantic and southwestern Pacific, our records also provide evidence for low oxygenation of deep waters, consistent with reduced overturning, which would have increased ocean carbon storage. Taken together our results highlight the complexities of carbon cycle feedback processes in the climate system.

Acknowledgements

We thank U. Röhl for generating the XRF data at Site 607. We thank T. Bickert for sharing the age model for Site 806, N. Exon and I.R. Hall for discussions about southwest Pacific oceanography, and Phil Meyers for informal reading of a draft and encouraging comments. We thank the editor Professor Wilson as well as one anonymous reviewer for their highly constructive feedback that has helped us to improve the manuscript. The first author would like to express gratitude to Wolf Berger, in memoriam, whose mentorship resulted in over 40 years of research using benthic foraminifera as a possible indicator of productivity. This study was funded by a grant from the Deutsche Forschungsgemeinschaft (DFG) DI472/13-1 to LDH. This research used samples provided by the Ocean Drilling Program (ODP) and the Deep Sea Drilling Project, now the International Discovery Program (IODP). IODP is sponsored by the U.S. National Science Foundation (NSF) and participating countries under the management of the Joint Oceanographic Institutions, Inc.

References

Alonso-Garcia, M., Sierro, F.J., Kucera, M., Flores, J.A., Cacho, I., Andersen, N., 2011. Ocean circulation, ice sheet growth and interhemispheric coupling of millennial climate variability during the mid-Pleistocene (ca 800–400 ka). Quat. Sci. Rev. 30, 3234–3247.

Antoine, D., Andre, J.-M., Morel, A., 1996. Oceanic primary production: 2. Estimation at global scale from satellite (coastal zone color scanner) chlorophyll. Glob. Biogeochem. Cycles 10, 57–69. http://dx.doi.org/10.1029/95GB02832.

Bassinot, F.C., Beaufort, L., Vincent, E., Labeyrie, L., 1997. Changes in the dynamics of western equatorial Atlantic surface currents and biogenic productivity at the "mid-Pleistocene revolution" (~930 ka). In: Proc. ODP, Sci. Result. 154. Ocean Drilling Program, College Station, TX, pp. 269–284.

Beaufort, L., de Garidel-Thoron, T., Mix, A.C., Pisias, N.G., 2001. ENSO-like forcing on oceanic primary production during the Late Pleistocene. Science 293, 2440–2443.

Becquey, S., Gersonde, R., 2002. Past hydrographic and climatic changes in the Subantarctic Zone of the South Atlantic — the Pleistocene record from ODP Site 1090. Palaeogeogr. Palaeoclimatol. Palaeoecol. 182, 221–239.

Berger, W.H., Wefer, G., 1990. Export production: seasonality and intermittency, paleoceanographic implications. Palaeogeogr. Palaeoclimatol. Palaeoecol. 89, 245–254.

Berner, R.A., 1984. Sedimentary pyrite formation: an update. Geochim. Cosmochim. Acta 48/4, 605–615.

Bickert, T., Berger, W.H., Burke, S., Schmidt, H., Wefer, G., 1993. Late Quaternary stable isotope record of benthic foraminifers: sites 805 and 806, Ontong Java Plateau. In: Proc. ODP, Sci. Results. 130. Ocean Drilling Program, College Station, TX, pp. 411–420. http://dx.doi.org/10.2973/odp.proc.sr.130.025.1993.

Bickert, T., Curry, W.B., Wefer, G., 1997. Late Pliocene to Holocene (2.6–0 Ma) western equatorial Atlantic deep-water circulation: inferences from benthic stable isotopes. In: Proc. ODP, Sci. Results. 154. Ocean Drilling Program, College Station, TX, pp. 239–254. http://dx.doi.org/10.2973/odp.proc.sr.154.110.1997.

Bolton, C.T., Lawrence, K.T., Gibbs, S.J., Wilson, P.A., Cleaveland, L.C., Herbert, T.D., 2010. Glacial-interglacial productivity changes recorded by alkenones and microfossils in the late Pliocene eastern equatorial Pacific and Atlantic upwelling zones. Earth Planet. Sci. Lett. 295, 401–411.

Boyd, P.W., Newton, P.P., 1999. Does planktonic community structure determine downward particulate organic carbon flux in different oceanic provinces? Deep-Sea Res. Part Oceanog. Res. Pap. 46, 63–91. http://dx.doi.org/10.1016/S0967-0637(98)00066-1.

Carter, R.M., McCave, I.N., Richter, C., Carter, L., et al., 1999. Proc. ODP, Init. Repts. 181 Ocean Drilling Program, College Station, TX. http://dx.doi.org/10.2973/odp.proc.ir.181.2000.

Charles, C.D., Froelich, P.N., Zibello, M.A., Mortlock, R.A., Morley, J.J., 1991. Biogenic opal in Southern Ocean sediments over the last 450,000 years: implications for surface water chemistry and circulation. Paleoceanography 6, 697–728.

Clark, P.U., Pollard, D., 1998. Origin of the middle Pleistocene transition by ice sheet erosion of regolith. Paleoceanography 13, 1–9. http://dx.doi.org/10.1029/97PA02660.

Clark, P.U., Archer, U.D., Pollard, D., Blum, J.D., Rial, J.A., Brovkin, V., Mix, A.C., Pisias, N.G., Roy, M., 2006. The middle Pleistocene transition: characteristics, mechanisms, and implications for long-term changes in atmospheric pCO_2. Quat. Sci. Rev. 25, 3150–3184.

Coale, K.H., Johnson, K.S., Chavez, F.P., 2004. Southern ocean iron enrichment experiment: carbon cycling in high- and low-Si waters. Science 304, 408–414.

Crundwell, M., Scott, G., Naish, T., Carter, L., Diekmann, B., 2008. Glacial–interglacial ocean climate variability from planktonic foraminifera during the Mid-Pleistocene transition in the temperate Southwest Pacific, ODP Site 1123. Palaeogeogr. Palaeoclimatol. Palaeoecol. 260, 202–229.

Curry, W.B., Shackleton, N.J., Richter, C., et al., 1995. Proc. ODP, Init. Repts. 154 Ocean Drilling Program, College Station, TX. http://dx.doi.org/10.2973/odp.proc.ir.154.1995.

Diekmann, B., Kuhn, G., 2002. Sedimentary record of the Mid-Pleistocene climate transition in the Southeastern Atlantic Ocean (ODP, Site 1090). Palaeogeogr. Palaeoclimatol. Palaeoecol (0031-0182(01)00498-9).

Diester-Haass, L., Schnitker, D., 1989. Plio-Pleistocene sedimentation regimes leading to chalk-marl cycles in the north Atlantic (DSDP Site 552, Hole 552A). Geol. Rundsch. 79, 959–985.

Diester-Haass, L., Meyers, P.A., Bickert, T., 2004. Carbonate crash and biogenic bloom in the Late Miocene: evidence from ODP Sites 1085, 1086 and 1087 in the Cape Basin, southeast Atlantic Ocean. Paleoceanography 19, PA1007. http://dx.doi.org/10.1029/2003PA000933.

Diester-Haass, L., Billups, K., Emeis, K.-C., 2006. Late Miocene carbon isotope records and marine biological productivity: was there a (dusty) link? Paleoceanography 21, PA4216. http://dx.doi.org/10.1029/2006PA001267.

Diester-Haass, L., Billups, K., Gröcke, D.R., François, L., Lefebvre, V., Emeis, K.-C., 2009. Mid Miocene paleoproductivity in the Atlantic Ocean and implications for the global carbon cycle. Paleoceanography 24, PA1209. http://dx.doi.org/10.1029/2008PA001605.

Diester-Haass, L., Billups, K., Emeis, K.-C., 2011. Marine biological productivity and carbon cycling during the Oligocene to Miocene climate transition. Palaeoecol. Palaeogeogr. Palaeoclimatol. 302, 464–473.

Diester-Haass, L., Billups, K., Jacquemin, I., Emeis, K.-C., Lefebvre, V., François, L., 2013. Paleoproductivity during the middle Miocene carbon isotope events: a data-model approach. Paleoceanography 28 (2), 334–346. http://dx.doi.org/10.1002/palo.20033.

Elderfield, H., Ferretti, P., Greaves, M., Crowhurst, S., McCave, I.N., Hodell, D., Piotrowski, A.M., 2012. Evolution of ocean temperature and ice volume through the mid-Pleistocene climate transition. Science 337 (6095), 704–709.

Farrell, J.W., Prell, W.L., 1999. Pacific $CaCO_3$ preservation and $\delta^{18}O$ since 4 Ma: paleoceanic and paleoclimatic implications. Paleoceanography 6 (4), 485–498. http://dx.doi.org/10.1029/91PA00877. (1991).

Ferretti, P., Shackleton, N.J., Rio, D., Hall, M.A., 2005. Early-Middle Pleistocene deep circulation in the western subtropical Atlantic: southern Hemisphere modulation of the North Atlantic Ocean. In: Head, M.J., Gibbard, P.L. (Eds.), Early-Middle Pleistocene Transitions: The Land Ocean Evidence. vol. 247. The Geol. Soc, London, U. K., pp. 131–145.

Francois, R., Honjo, S., Krishfield, R., Manganini, S., 2002. Factors controlling the flux of organic carbon to the bathypelagic zone of the ocean. Glob. Biogeochem. Cycles 16 (4), 1087. http://dx.doi.org/10.1029/2001GB001722.

Gersonde, R., Hodell, D.A., Blum, P., et al., 1999. Proc. ODP, Init. Repts. 177 Ocean Drilling Program, College Station, TX. http://dx.doi.org/10.2973/odp.proc.ir.177.1999.

Hall, I.R., McCave, I.N., Shackleton, N.J., Weedon, G.P., Harris, S.E., 2001. Intensified deep Pacific inflow and ventilation in Pleistocene glacial times. Nature 412, 809–812.

Hays, J.D., Imbrie, J., Shackleton, N.J., 1976. Variations in the Earth's orbit: pacemaker of the ice ages. Science 194 (4270), 1121–1132.
Herbert, T.D., Peterson, L.C., Lawrence, K.T., Liu, Z., 2010. Tropical ocean temperatures over the past 3.5 million years. Science 328 (5985), 1530–1534.
Herguera, J.C., 2000. Last glacial paleoproductivity patterns in the eastern equatorial Pacific: benthic foraminifera records. Mar. Micropaleontol. 40, 259–275. http://dx.doi.org/10.1016/S0377-8398(00)00041-4.
Herguera, J.C., Berger, W.A., 1991. Paleoproductivity from benthic foraminifera abundance: glacial to postglacial change in the west-equatorial Pacific. Geology 19, 1173–1176. http://dx.doi.org/10.1130/0091-7613(1991)019<1173:PFBFAG>2.3.CO;2.
Hernandez-Almeida, I., Bjoklund, K.R., Sierro, F.J., Filippelli, G.M., Cacho, I., Flores, J.A., 2013. A high resolution opal and radiolarian record from the subpolar North Atlantic during the Mid-Pleistocene Transition (1069–779 ka): paleoceanographic implications. Palaeogeogr. Palaeoclimatol. Palaeoecol. 391, 49–70. http://dx.doi.org/10.1016/j.palaeo.2011.05.049.
Hesse, P.P., 1994. The record of continental dust from Australia in Tasman Sea sediments. Quat. Sci. Rev. 13, 257–272.
Hodell, D.A., Venz-Curtis, K.A., 2006. Late Neogene history of deepwater ventilation in the Southern Ocean. Geochem. Geophys. Geosyst. 7, Q09001. http://dx.doi.org/10.1029/2005GC001211.
Hogg, N.G., Jones, W.E., 1995. Western boundary current. Rev. Geophys. 1311–1334.
Hönisch, B., Hemming, N.G., Archer, D., Siddall, M., McManus, J.F., 2009. Atmospheric carbon dioxide concentration across the mid-Pleistocene transition. Science 324, 1551–1554. http://dx.doi.org/10.1126/science.1171477.
Howell, P., 2012. ARAND Time Series and Spectral Analysis Package for the Macintosh. Brown University.
Imbrie, J., et al., 1993. On the structure and origin of major glacial cycles. Part 2. The 100,000-year cycle. Paleoceanography 8, 699–736. http://dx.doi.org/10.1029/93PA02751.
Karas, C., Nürnberg, D., Gupta, A.K., Tiedemann, R., Mohan, K., Bickert, T., 2009. Mid-Pliocene climate change amplified by a switch in Indonesian subsurface throughflow. Nat. Geosci. 2, 434–438. http://dx.doi.org/10.1038/ngeo520.
Knies, J., Matthiessen, J., Vogt, C., Laberg, B., Hjelstuen, O., Smelror, M., Larsen, E., Andreassen, K., Eidvin, T., Vorren, T.O., 2009. The Plio-Pleistocene glaciation of the Barents Sea-Svalbard region: a new model based on revised chronostratigraphy. Quat. Sci. Rev. 28, 812–829.
Kroenke, L.W., Berger, W.H., Janecek, T.R., et al., 1991. Proc. ODP, Init. Repts. 130 Ocean Drilling Program, College Station, TX. http://dx.doi.org/10.2973/odp.proc.ir.130.1991.
Lampitt, R.S., Anita, A.M., 1997. Particle flux in deep seas: regional characteristics and temporal variability. Deep-Sea Res. I Oceanogr. Res. Pap. 44, 1377–1403.
Lamy, F., Gersonde, R., Winckler, G., Esper, O., Jaeschke, A., Kuhn, G., Ullermann, J., Martinez-Garcia, A., Lambert, F., Kilian, R., 2014. Increased dust deposition in the Pacific Southern Ocean during glacial periods. Science 343, 403–407.
Lang, D.C., Bailey, I., Wilson, P.A., Beer, C.J., Bolton, C.T., Friedrich, O., Newsam, C., Spencer, M.R., Gutjahr, M., Foster, G.L., Cooper, M.J., Milton, J.A., 2014. The transition on North America from the warm humid Pliocene to the glaciated Quaternary traced by eolian dust deposition at a benchmark North Atlantic Ocean drill site. Quat. Sci. Rev. 93, 125–141.
Lang, D., Bailey, I., Wilson, P.A., Chalk, T.B., Foster, G.L., Gutjahr, M., 2016. Incursions of southern-sourced water into the deep North Atlantic during late Pliocene glacial intensification. Nat. Geosci. 9. http://dx.doi.org/10.1038/NGEO2688.
Lawrence, K.T., Sosdian, S., White, H.E., Rosenthal, Y., 2010. North Atlantic climate evolution through the Plio-Pleistocene climate transitions. Earth Planet. Sci. Lett. 300, 329–342. http://dx.doi.org/10.1016/j.epsl.2010.10.013.
Lawrence, K.T., Sigman, D.M., Herbert, T.D., Riihimaki, C.A., Bolton, C.T., Martinez-Garcia, A., Rosell-Mele, A., Haug, G.H., 2013. Time transgressive North Atlantic productivity changes upon Northern Hemisphere glaciation. Paleoceanography 28, 740–751. http://dx.doi.org/10.1002/2013PA002546.
Lazarus, D., Bittniok, B., Diester-Haass, L., Meyers, P., Billups, K., 2006. Comparison of radiolarian and sedimentologic paleoproductivity proxies in the latest Miocene-Recent Benguela Upwelling System. Mar. Micropaleontol. 60, 269–294.
Lazarus, D., Bittniok, B., Diester-Haass, L., Billups, K., Ogaway, Y., Takahashi, K., Meyers, P., 2008. Radiolarian and sedimentologic paleoproductivity proxies in late Pleistocene sediments of the Benguela Upwelling System, ODP Site 1084. Mar. Micropaleontol. 68, 223–235.
Lea, D.W., Pak, D.K., Spero, H.J., 2000. Climate impact of Late Quaternary equatorial Pacific sea surface temperature variations. Science 289, 1719–1724.
Lear, C.H., Billups, K., Rickaby, R.E.M., Diester-Haass, L., Mawbey, E.M., Sosdian, S.M., 2016. Breathing more deeply: deep ocean carbon storage during the mid-Pleistocene climate transition. Geology 44, 12. http://dx.doi.org/10.1130/G38636.1.
Lee, J., Shackleton, N.J., 1992. Carbonate dissolution fluctuations in the western equatorial Pacific during the Late Quaternary. Paleoceanography 7, 21–42.
Lisiecki, L., 2010. A simple mixing explanation for late Pleistocene changes in the Pacific-South Atlantic benthic ^{13}C gradient. Clim. Past 6, 305–314.
Lisiecki, L.E., Raymo, M.E., 2005. A Pliocene-Pleistocene stack of 57 globally distributed benthic $\delta^{18}O$ records. Paleoceanography 20, PA1003. http://dx.doi.org/10.1029/2004PA001071.
Liu, Z., Herbert, T.D., 2004. High-latitude influence on the eastern equatorial Pacific climate in the early Pleistocene epoch. Nature 427 (6976), 720–723.
Lüer, V., Hollis, C.J., Willem, H., 2008. Late Quaternary radiolarian assemblages as indicators of paleoceaonographic changes north of the subtropical front, offshore eastern New Zealand, southwest Pacific. Micropaleontology 54, 49–69.
Lüthi, D., et al., 2008. High-resolution carbon dioxide concentration record 650,000–800,000 years before present. Nature 453, 379–382. http://dx.doi.org/10.1038/nature06949.
Lutze, G.F., 1980. Depth distribution of benthic foraminifera on the continental margin off northwest Africa. "Meteor" Forschungsergebnisse 32, 31–80 Reihe C.
Lutze, G.F., Coulbourn, W.T., 1984. Recent benthic foraminifera from the continental margin of northwest Africa- community structure and distribution patterns. Mar. Micropaleontol. 8, 361–401.
Lyle, M.W., Zahn, R., Prahl, F.G., Dymond, J.R., Collier, R.W., Pisias, N.G., Suess, E., 1992. Paleoproductivity and carbon burial across the California current: the multi-tracer transect 42°N. Paleoceanography 7 (3), 251–272. http://dx.doi.org/10.1029/92PA00696.
Ma, Z., Ravelo, A.C., Liu, Z., Zhou, L., Paytan, A., 2015. Export production fluctuations in the eastern equatorial Pacific during the Pliocene-Pleistocene: reconstruction using barite accumulation rates. Paleoceanography 30 (11), 1455–1469. http://dx.doi.org/10.1002/2015PA002860.
Marino, M., Maiorano, P., Flower, B.P., 2011. Calcareous nannofossil changes during the Mid-Pleistocene Revolution; paleoecologic and paleoceanographic evidence from North Atlantic Site 980/981. Palaeogeogr. Palaeoclimatol. Palaeoecol. 306, 58–69.
Martin, John H., 1990. Glacial-interglacial CO_2 change: the iron hypothesis. Paleoceanography 5 (1), 1–13.
Martinez-Garcia, A., Rosell-Mele, A., Geibert, W., Gersonde, R., Masque, P., Gaspari, V., Barbante, C., 2009. Links between iron supply, marine productivity, sea surface temperature, and CO_2 over the last 1.1 Ma. Paleoceanography 24, PA1207. http://dx.doi.org/10.1029/2008PA001657.
Martinez-Garcia, A., Rosell-Mele, A., McClymont, E.L., Gersonde, R., Haug, G., 2010. Subpolar link to the emergence of the modern equatorial Pacific cold tongue. Science 328, 1550–1553.
Martinez-Garcia, A., Rosell-Mele, A., Jaccard, S.L., Geibert, W., Sigman, D.M., Haug, G.H., 2011. Southern Ocean dust-climate coupling over the past four million years. Nature 476, 312–316. http://dx.doi.org/10.1038/nature10310.
Mayer, L., Pisias, N., Janecek, T., et al., 1992. Proc. ODP, Init. Repts. 138 Ocean Drilling Program, College Station, TX. http://dx.doi.org/10.2973/odp.proc.ir.138.1992.
McClymont, E.L., Rosell-Mele, A., Haug, G.H., Lloyd, J.M., 2008. Expansion of subarctic water masses in the North Atlantic and Pacific oceans and implications for mid-Pleistocene ice sheet growth. Paleoceanography 23, PA4214. http://dx.doi.org/10.1029/2008PA001622.
McClymont, E.L., Sosdian, S., Rosell-Mele, A., Rosenthal, Y., 2013. Pleistocene sea-surface temperature evolution: early cooling, delayed glacial intensification, and implications for the mid-Pleistocene climate transition. Earth-Sci. Rev. 123, 173–193. http://dx.doi.org/10.1016/j.earscirev.2013.1004.1006.
McIntyre, A., Molfino, B., 1996. Forcing of Atlantic equatorial and subpolar millennial cycles by precession. Science 274, 1867–1870.
Miller, K.G., Lohmann, G.P., 1982. Environmental distribution of recent benthic foraminifera on the northeast United States continental slope. Geol. Soc. Am. 93, 200–206.
Mix, A.C., Pisias, N.G., Rugh, W., Wilson, J., Morey, A., Hagelberg, T.K., 1995. Benthic foraminifer stable isotope record from Site 849 (0–5 Ma): local and global climate changes. In: Proc. ODP leg138, Scientific Results, College Station, TX, pp. 371–412. http://dx.doi.org/10.2973/odp.proc.sr.138.120.1995.
Mudelsee, M., Schulz, M., 1997. The Mid-Pleistocene climate transition: onset of 100 ka cycle lags ice volume build-up by 280 ka. Earth Planet. Sci. Lett. 151 (1–2), 117–123.
Murray, R.W., Leinen, M., Knowlton, C.W., 2012. Links between iron input and opal deposition in the Pleistocene equatorial Pacific Ocean. Nat. Geosci. 5 (4), 270–274.
Naafs, B.D.A., Stein, R., Hefter, J., Khélifi, N., De Schepper, S., Haug, G.H., 2010. Late Pliocene changes in the North Atlantic current. Earth Planet. Sci. Lett. 298, 434–442.
Naafs, B.D.A., Hefter, J., Acton, G., Haug, G.H., Martinez-Garcia, A., Pancost, R., Stein, R., 2012. Strengthening of North American dust sources during the late Pliocene (2.7 Ma). Earth Planet. Sci. Lett. 317–318, 8–19.
Nees, S., 1997. Late Quaternary palaeoceanography of the Tasman Sea: the benthic foraminiferal view. Palaeogeogr. Palaeoclimatol. Palaeoecol. 131, 365–389. http://dx.doi.org/10.1016/S0031-0182(97)00012-6.
Paytan, A., Kastner, M., Chavez, F., 1996. Glacial to interglacial fluctuations in productivity in the equatorial Pacific as indicated by marine barite. Science 274, 1355–1357.
Pena, L.D., Goldstein, S.L., 2014. Thermohaline circulation crisis and impacts during the mid-Pleistocene transition. Science 345, 318–322. http://dx.doi.org/10.1126/science.1249770.
Philander, S.G.H., Pacanowski, R.C., 1986. A model of the seasonal cycle in the tropical Atlantic Ocean. J. Geophys. Res. 91 (C12), 14192–14206. http://dx.doi.org/10.1029/JC091iC12.
Poirier, R.K., Billups, K., 2014. The intensification of northern component deep water formation during the mid-Pleistocene climate transition. Paleoceanography 29, 1046–1061. http://dx.doi.org/10.1002/2014PA002661.
Raymo, M.E., Ruddiman, W.F., Shackleton, N.J., Oppo, D.W., 1990. Evolution of Atlantic-Pacific $\delta^{13}C$ gradients over the last 2.5 m.y. Earth Planet. Sci. Lett. 97, 353–368. http://dx.doi.org/10.1016/0012-821X(90)90051-X.
Rea, D.K., Pisias, N.G., Newburry, T., 1991. Late Pleistocene paleoclimatology of the central equatorial Pacific: flux patterns of biogenic sediments. Paleoceanography 6, 227–244.
Roberts, D.G., Schnitker, D., et al., 1984. Init. Repts. DSDP. 81 U.S. Govt. Printing Office, Washington.
Ruddiman, W.F., McIntyre, A., 1981. The mode and mechanism of the last deglaciation: oceanic evidence. Quat. Res. 16 (2), 125–134.
Ruddiman, W.F., McIntyre, A., Raymo, M.E., 1986. Paleoenvironmental Results From North Atlantic Sites 607 and 609. Initial Reports DSDP. vol. 94. pp. 855–878.
Ruddiman, W.F., Kidd, R.B., Thomas, E., et al., 1987. Init. Repts. DSDP. 94 U.S. Govt. Printing Office, Washington.

Sarmiento, J.L., Gruber, N., Brezinski, M.A., Dunne, J.P., 2004. High-latitude controls of thermocline nutrients and low latitude biological productivity. Nature 427, 56–60.
Schmieder, F., von Dobenek, T., Bleil, U., 2000. The Mid-Pleistocene climate transition as documented in the deep South Atlantic Ocean: initiation, interim state and terminal event. Earth Planet. Sci. Lett. 179 (3–4), 539–549. http://dx.doi.org/10.1016/S0012-821X(00)00143-6.
Schmiedl, G., Mackensen, A., 1997. Late Quaternary paleoproductivity and deep water circulation in the eastern South Atlantic Ocean: evidence from benthic foraminifera. Palaeogeogr. Palaeoclimatol. Palaeoecol. 130, 43–80. http://dx.doi.org/10.1016/S0031-182(96)00137-X.
Sexton, Philip F., Barker, S., 2012. Onset of 'Pacific-style' deep-sea sedimentary carbonate cycles at the mid-Pleistocene transition. Earth Planet. Sci. Lett. 321-322, 81–94.
Stein, R., Hefter, J., Grützner, J., Voelker, A., Naafs, B.D.A., 2009. Variability of surface water characteristics and Heinrich-like events in the Pleistocene mid-latitude North Atlantic Ocean: biomarker and XRD records from IODP Site U1313 (MIS 16-9). Paleoceanography 24, PA2203. http://dx.doi.org/10.1029/2008PA001639.
Takahashi, K., 1987. Radiolarian flux and seasonality: climatic and El Nino response in the subarctic Pacific. Glob. Biogeochem. Cycles 1, 213–231.
Toggweiler, J.R., Dixon, K., Broecker, W.S., 1991. The Peru upwelling and the ventilation of the South Pacific thermocline. J. Geophys. Res. 96, 20467–20497.
Trick, C.G., Bill, B.D., Cochlan, W.P., Wells, M.L., Trainer, V.L., Pickell, L.D., 2017. Iron enrichment stimulates toxic diatom production in high-nitrate, low-chlorophyll areas. PNAS 107/13, 5887–5892. http://dx.doi.org/10.1073/pnas.0910579107.
Tzedakis, P.C., Crucifix, M., Mitsui, T., Wolff, E.W., 2017. A simple rule to determine which insolation cycles lead to interglacials. Nature 542, 427–432.
Waite, A., Diester-Haass, L., Gibbs, S., Rickaby, R., Billups, K., 2008. A top-down and bottom-up comparison of paleoproductivity proxies: calcareous nannofossil Sr/Ca ratios and benthic foraminiferal accumulation rates. G-Cube 9. http://dx.doi.org/10.1029/2007GC001812.
Winckler, G., Anderson, R.F., Robert, F., Fleisher, M.Q., McGee, D., Mahowa, N., 2008. Covariant glacial-interglacial dust fluxes in the Equatorial Pacific and Antarctica. Science 320, 93–96.
Wolff, E.W., Chappellaz, J., Blunier, T., Rasmussen, S.O., Svensson, A., 2010. Millennial-scale variability during the last glacial: the ice core record. Quat. Sci. Rev. 29, 2828–2838.
Xu, Z., Li, T., Clift, P.D., Lim, D., Wan, S., Chen, H., Tang, Z., Jiang, F., Xiong, Z., 2015. Quantitative estimates of Asian dust input to the western Philippine Sea in the mid late Quaternary and its potential significance for paleoenvironment. Geochem. Geophys. Geosyst. 16, 3182–3196. http://dx.doi.org/10.1002/2015GC005929.
Yasuda, H., 1997. Late Miocene-Holocene paleoceanography of the western equatorial Atlantic: evidence from deep-sea benthic foraminifera. Proc. ODP Sci. Results 154, 395–432.
Yasuda, M., Berger, W.H., Wu, G., Burke, S., Schmidt, H., 1993. Foraminifer preservation record for the last million years: Site 805, Ontong Java Plateau. In: Proc. ODP, Sci. Results. 130. Ocean Drilling Program, College Station, TX, pp. 491–503. http://dx.doi.org/10.2973/odp.proc.sr.130.008.1993.
van der Zwaan, G.J., Duijnstee, I.A.P., den Bulk, M., Ernst, S.R., Jannink, N.T., Kouwenhoven, T.J., 1999. Benthic foraminifers: proxies or problems? A review of paleoecological concepts. Earth Sci. Rev. 46, 213–236. http://dx.doi.org/10.1016/S0012-8252(99)00011-2.
Venz, K.A., Hodell, D.A., 2002. New evidence for changes Plio-Pleistocene record of deepwater circulation in the Southern Ocean from ODP Leg 177 site 1090. Palaeogeogr. Palaeoclimatol. Palaeoecol (0031-0182(01)00496-5).